# Influence of ENSO and of the Indian Ocean Dipole on the Indian summer monsoon variability

Annalisa Cherchi[1] and Antonio Navarra[1]

[1]Centro Euromediterraneo per i Cambiamenti Climatici, and Istituto Nazionale di Geofisica e Vulcanologia, Bologna, Italy

Manuscript submitted to

**Climate Dynamics**

November 8, 2012

**Corresponding author:**
Annalisa Cherchi (CMCC/INGV)
Viale Aldo Moro 44
40127 Bologna, Italy
E-mail: annalisa.cherchi@bo.ingv.it
Phone: +39 051 3782613
Fax: +39 051 3782655

## Abstract

Indian summer monsoon (ISM) variability is forced from external factors (like the El Niño Southern Oscillation, ENSO) but it contains also an internal component that tends to reduce its potential for predictability. Large-scale and local monsoon indices based on precipitation and atmospheric circulation parameters are used as a measure of ISM variability. In a 9-members ensemble of AMIP-type experiments (with same boundary SST forcing and different initial conditions) their potential predictability is comparable using both local and large-scale monsoon indices. In the sample analyzed, about half of more predictable monsoon years coincide with El Niño and/or positive Indian Ocean Dipole (IOD) events.

Summer monsoon characteristics during ENSO and IOD years are analyzed through composites computed over a three years period (i.e. one year before and one year after the event peak) to investigate the mutual relationship between the events lagged in time. The connection between ISM and IOD is mostly confined in the summer and autumn, while that with ENSO is stronger and extends more in time. In the coupled model results the IOD influence on the monsoon is large, even because in the model IOD events are intense and easily reproduced due to a strong air-sea feedback in the eastern side of the basin. Monsoon seasons preceding or following an El Niño or a La Niña event are not exactly symmetric, even in terms of their biennial character. In most of the cases, both in reanalysis and model, El Niño and positive IOD events tend to co-occur with larger anomalies either in the Indo-Pacific ocean sector or over India, while La Niña and negative IOD do not.

From the observed record, the ENSO-IOD correlation is positive strong and significant since mid-60s and it may correspond with either strong or

weak ENSO-monsoon relationship and with strong or weak IOD-monsoon relationship.  A main difference between those periods is the relationship between Indian monsoon rainfall and SST in other ocean basins rather than the Indo-Pacific sector alone.

# 1 Introduction

The Indian summer monsoon (ISM) is one of the main components of the broad-scale Asian summer monsoon that represents the largest source of moisture and precipitation of the tropical sector (Webster et al., 1998). The ISM varies at many timescales, from intra-seasonal to interdecadal, and it is largely modulated by external factors, like the El Niño Southern Oscillation (ENSO). This remote influence is known since the beginning of the 19th century and it has been widely investigate in the past (Walker, 1924; Sikka, 1980; Rasmusson and Carpenter, 1983; Kirtman and Shukla, 2000, among others). The negative relationship between ENSO and the ISM can be explained as a modulation of the Walker circulation (i.e. Ju and Slingo, 1995). During warm ENSO episodes, the rising limb of the Walker circulation shifts eastward in response to a warming of the eastern Pacific causing descent of air in the Western Pacific and Indian sectors with decreased monsoon rainfall (Goswami, 1998; Lau and Wang, 2006).

The dependence of the ISM variability on ENSO, i.e. on the remote SST forcing from the Pacific Ocean, represents a very important aspect of the monsoon for its prediction. In a general perspective, the understanding that anomalous boundary conditions provide potential predictability is the scientific basis for deterministic climate predictions (Charney and Shukla, 1981). Monsoon predictability is indeed a crucial issue as life and economy of million of people depends on its rainfall, but because of its complex nature and the diversity of its interactions, useful monsoon prediction is still a challenge (Webster and Hoyos, 2010; Turner and Annamalai, 2012). In the Asian/Indian monsoon regions, both externally forced and internal variability components have been identified to measure the monsoon potential predictability (Shukla, 1981; Singh and Kripalani, 1986; Goswami, 1998; Mohan and Goswami, 2003, among others). Because of the determining role of the internal ”unpredictable” variability component, some studies tried as well to link it to the monsoon intra-seasonal oscillation (Goswami, 1994; Sperber et al., 2000; Goswami and

Xavier, 2005).

Toward the end of the 20th century changes have been documented in the strength of the ENSO-monsoon relationship (Kumar et al., 1999; Kinter et al., 2002). Even though studies suggested that its weakening could be apparent, as either due to the use of fixed definition of seasons (Xavier et al., 2007), or to random fluctuations (van Oldenborgh and Burgers, 2005). In the last two decades, the Indian Ocean Dipole (IOD, Saji et al., 1999; Webster et al., 1999) has been identified as potential trigger of the ENSO-monsoon connection (Ashok et al., 2001; Li et al., 2003), but its active or passive role has not been clearly identified yet (Webster et al., 2002; Meehl et al., 2003; Wu and Kirtman, 2004; Cherchi et al., 2007). Air-sea interaction processes in the Indian Ocean are undoubtedly involved in the monsoon dynamics; hence they are crucial for the ENSO-monsoon teleconnection (Wu and Kirtman, 2004; Shinoda et al., 2004; Bracco et al., 2007).

On interannual timescales, a large component of the Asian summer monsoon variability consists of its biennial character, with a relatively strong event that tends to be followed by a relatively weak one in the next year. This variability has been identified as the tropospheric biennial oscillation (TBO; Meehl, 1994, 1997). The biennial character of the tropical climate in the Indian and Pacific regions largely involves the Indian summer monsoon, ENSO, Indian Ocean dynamics and their mutual interactions (Meehl et al., 2003; Wu and Kirtman, 2007). Shifting of large-scale east-west circulation, Rossby wave type response and surface heat fluxes-SST feedback are at the base of the ENSO influence on the ISM biennial variations (Meehl et al., 2003). North Indian Ocean SST anomalies (SSTA) contribute as well to rainfall transitions via anomalous low-level moisture convergence (Wu and Kirtman, 2007). IOD, ENSO, the monsoon and their mutual connections form an important and complex aspect of the tropical climate worth of further attention (Tamura et al., 2011; Boschat et al., 2011; Pokhrel et al., 2012; Achuthavarier et al., 2012).

In the present study we intend to contribute to the understanding of the relationship between the Indian summer monsoon, ENSO and the Indian Ocean dipole. In particular, we explore how the Indian summer monsoon characteristics are influenced by ENSO and IOD events, focusing on the biennial character of the monsoon. As previously mentioned, this is one of the regions where the air-sea interaction is crucial (Wu and Kirtman, 2004; Bracco et al., 2007). Nevertheless, atmospheric forced experiments can still be useful to understand aspects of the monsoon dynamics and variability, particularly when they can be compared with coupled model simulations. In this study, an ensemble of AMIP-type experiments, with forced SST boundary conditions, and an ocean-atmosphere coupled model experiment are analyzed and compared with available data and reanalysis. The role of the IOD-ENSO relationship in the weakening/strengthening of the ENSO-monsoon connection is questioned as well. In the AMIP-type ensemble we are also interested in measuring the potential predictability of monsoon precipitation and circulation-based indices coming from Pacific and Indian Ocean SST.

The study is organized as follows: Section 2 describes the experiments analyzed (including the models used to produce them), and it lists datasets and reanalysis included in the study and in the model experiments comparison. Section 3 is dedicated to the description of the mean state and variability over India in terms of monsoon indices, including the analysis of the potential predictability of monsoon extreme years in the AMIP-type ensemble. Section 4 compares the monsoon characteristics during ENSO and IOD years in both model results and reanalysis. Section 5 is mainly focused on the study of the changes occurring in the ENSO-monsoon relationship and it is mostly based on the atmospheric reanalysis. Finally, Section 6 collects the main conclusions of the study.

## 2 Model, experiments and datasets

Two kinds of experiments have been used for the present study: an AMIP-type ensemble and a 20th century coupled model experiment. The AMIP-type ensemble consists of 9 members with the same boundary, but different initial conditions. The boundary conditions are interannually varying SST taken from the HadISST dataset (Rayner et al., 2003). The time record analyzed is 1948-2003. The experiments have been performed with the ECHAM4 atmospheric model (Roeckner et al., 1996) at T106 horizontal resolution (roughly corresponding to 1x1 spatial grid) and 19 vertical sigma levels.

The twentieth century simulation has been performed with the fully coupled atmosphere-ocean general circulation model SINTEXG (Gualdi et al., 2008). It includes prescribed concentration of greenhouse gases (i.e. $CO_2$, $CH_4$ $N_2O$ and chloro-fluoro-carbons) and sulfate aerosols, as specified for the 20C3M experiment defined for the IPCC AR4 simulations (see http://www-pcmdi.llnl.gov/ipcc/about_ipcc.php for more details) from 1901 to 2000. The characteristics of both atmospheric and oceanic model components are described in previous publications (Cherchi et al., 2008; Gualdi et al., 2008). The atmospheric component is the same used for the AMIP-type ensemble and at the same resolution, while the oceanic component is OPA (Madec et al., 1998), which is spatially distributed over a three-dimensional Arakawa-C-type grid (about $2^\circ \times 2^\circ$ horizontal resolution, with a meridional refinement of $0.5^\circ$ at the Equator, and 31 prescribed vertical levels).

The model outputs have been compared with observations and re-analysis data. In particular, the global distribution of sea surface temperature has been taken from the HadISST dataset over a 1x1 grid (Rayner et al., 2003), atmospheric fields come from the NCEP reanalysis (Kalnay et al, 1996) in a regular 2.5x2.5 grid, and the global precipitation over land at 0.5x0.5 resolution is taken from the CRU dataset (Mitchell and Jones, 2005). Satellite globally distributed precipitation for the period 1979-2006 over a 2.5 regular grid from the CMAP dataset (Xie and Arkin, 1997) has been used as well. Observed datasets are used in their original grid, except when compared directly. In that case data are interpolated over a common grid, usually the coarser one.

## 3 Mean state and variability: Monsoon indices

Fig. 1 shows the annual cycle of the precipitation and of the zonal wind shear (as U850 minus U200) zonally averaged over the Indian monsoon region (between 60-90E). Both forced and coupled model performance is realistic: large amounts of precipitation move from the ocean toward the land in summer, but the maximum remains over the ocean, as is observed (fig. 1). The comparison between AMIP-type and coupled model experiments reveals that when oceanic and atmospheric components are coupled (i.e. they can exchange fluxes), the model performance improves with an increase (decrease) of land (ocean) precipitation (fig. 1a,b). The zonal wind shear (contours in fig. 1) is used to represent the mean circulation over the Indian monsoon region (Webster and Yang, 1992). The model simulation is realistic with zonal wind shear maxima in summer at 10N, but in the coupled model experiment the values are slightly weaker than observed (fig. 1c).

Fig. 2 summarizes the summer mean state in terms of SST, precipitation and upper troposphere velocity potential, and it shows the main biases of the model. The model, both forced and coupled, has less than observed precipitation over India and in the Bay of Bengal (fig. 2a,b,c shaded contours). Over the Indian Ocean the precipitation bias in the western basin is reduced in the coupled model, thanks to the contribution of the air-sea interaction (Cherchi and Navarra, 2007). On the other hand, in the eastern side the coupled model bias is larger than in the AMIP-type ensemble because of the cold SST bias (fig. 2d).

In the Pacific Ocean, the simulated SST is colder than observed, with the cold tongue extending farther east (fig. 2d). In that area, precipitation is largely underestimated (fig. 2d) and it shows the typical coupled model double ITCZ syndrome (Bellucci et al., 2010). The upper troposphere velocity potential is realistically centered over the Asian continent in the model (fig. 2, contours), even if the intensity is much weaker in the coupled model where it reflects the weaker than observed low-level convergence (fig. 2c).

The Indian monsoon intensity and variability may be expressed in terms of the summer (JJA) mean rainfall averaged over India (IMR - Indian monsoon rainfall index). The definition and usage of this index follow the All-Indian Rainfall (AIR) values obtained from rain-gauges measurements as described in Parthasarathy et al. (1992). In the AMIP-type ensemble, the IMR index computed for the ensemble mean is significantly correlated with the CRU dataset, and the value is 0.44, indicating that the portion of ISM variability externally forced is large. As the ensemble mean removes the internal variability, its correlation with the observations is larger than if considering the value for each member of the ensemble, or their average.

The relationship between summer precipitation over India, IOD and ENSO is lagged in time (i.e. Turner et al., 2007; Izumo et al., 2010; Boschat et al., 2011). Fig. 3 shows the lagged correlation between IMR, ENSO and IOD in terms of SST anomalies. In particular, ENSO and IOD are measured here in terms of SST anomalies using the NINO3 and the IODM indices, respectively. NINO3 is the average of monthly mean SST anomalies in the area 150-90W 5S-5N, while IODM is the monthly SST anomalies difference between a western (60-80E, 10S-10N) and an eastern (90-110E, 10S-Eq) box in the Indian Ocean (Saji et al., 1999; Saji and Yamagata, 2003). In the reanalysis and in the AMIP-type ensemble, the correlation between IMR and NINO3 is negative and significant starting before the summer, it peaks in July, in the core of the monsoon season, and it remains negative and large after the monsoon peak (fig. 3a,b). On the other hand, the correlation between IMR and IODM in the re-analysis is negative and significant only during the fall after the monsoon peak (fig. 3a - dashed line). If the eastern and western poles of the IOD are considered separately, the western side has the largest correlation (not shown). In the AMIP-type ensemble, the correlation is negative and significant during the whole monsoon season (fig. 3b, dashed line) and as in the re-analysis the main connection is through the western lobe of the dipole (not shown). According to this result, while the ENSO-monsoon relationship appears strong during the developing phase of ENSO, the IOD-monsoon connection is mostly confined to the monsoon demise phase, corresponding to the peak of the evolution of the Indian Ocean Dipole. In the period 1979-2007 the correlation between Indian summer monsoon rainfall and fall IOD index is significant only in September (Boschat et al., 2011).

IMR is an example of a widely used index to measure the monsoon variability. However, it is well recognized that models tend to better simulate the monsoon in terms of circulation fields than in terms of precipitation. In fact, in literature many different indices based on circulation parameters have been defined and used (Webster and Yang, 1992; Kawamura, 1998; Wang and Fan, 1999; Wang et al., 2001, among others). Fig. 4 shows the annual cycle of four different indices: the precipitation-based index IMR is compared with three circulation-based indices, computed in the reanalysis and in the model experiments. In terms of precipitation averages, as previously mentioned, the model experiments tend to have less precipitation than observed over the Indian subcontinent (fig. 4a). In the coupled model the amount of precipitation in summer is more realistic but the time extension is wider than observed (it seems that the onset is slightly anticipated while the demise is slightly delayed). Fig. 4b shows the Indian Monsoon Index (IMI) defined by Wang et al. (2001). This index is computed as 850 mb JJA zonal wind difference between two sectors over the Indian monsoon region (i.e. 40-80E, 5-15N minus 70-90E, 20-30N), and it has been recognized as a good index to represent the Indian monsoon variability in the coupled model used in this study (Cherchi et al., 2007). In terms of intensity the index is slightly underestimated in the experiments, but it has a realistic time evolution during the year (fig. 4b).

The indices just described are mostly local, but ISM variability may be represented in terms of large-scale features as well. According to that, Webster and Yang (1992) introduced the Dynamical Monsoon Index (DMI) defined as the zonal wind shear between lower and upper troposphere (U850 minus U200) averaged in the region 40-110E, Eq-20N. Fig. 4c shows how the AMIP-type ensemble is able to realistically simulate its annual cycle, while the coupled model simulation tends to underestimate its intensity, as already discussed for fig. 1. Another large-scale index is the MTG (Meridional Temperature Gradient) defined by Kawamura (1998) as the atmospheric thickness (geopotential height difference between 200 and 500 mb) difference between 50-100E, Eq-20N and 50-100E, 20-40N in summer. The MTG index is strictly connected with the zonal wind shear changes and it contains details of the atmospheric thickness associated with intense monsoon convection (Kawamura, 1998). Fig. 4d shows how the model experiments simulate its annual cycle in a realistic way. The variability of the large-scale monsoon indices is better represented compared to local indices. In fact, in the AMIP-type ensemble MTG and DMI are highly correlated with the indices computed from NCEP. The correlation coefficients considering the ensemble mean are 0.70 and 0.58, respectively.

In literature many other indices have been introduced, based on meridional wind shear (Wang and Fan, 1999) or 200mb velocity potential (Tanaka et al., 2004), to represent the Hadley and the Walker type circulations, respectively, over the area. However, for the purpose of this study and building on a previous study discussion on the performance of the same model (Cherchi and Navarra, 2007), we evaluate the indices shown in fig. 4 as appropriate to represent the ISM variability.

Considering the availability of nine members in the ensemble, for each index we compute the potential predictability for each year and we compare the performances. As mentioned in the Introduction the concept of potential predictability has been widely investigated in the 90's and it can be measured as a sort of signal to noise ratio (i.e. Stern and Miyakoda, 1995). In particular, the signal relies on the forcing from the SST (i.e. ensemble mean), while the noise is represented in terms of the internal component (i.e. spread among the ensemble). The signal to noise ratio as measure of the potential predictability coming from the SST forcing has been studied as well using the analysis of variance (ANOVA) statistical technique in ensembles of GCM experiments (Rowell, 1998). Tropical precipitation is largely controlled by the given SST distribution, specifically in the ENSO sector (Kang et al, 2004), while in the ISM region internal oscillations can account for a large fraction of the simulated monsoon variability (Goswami, 1998; Krishnamurthy and Shukla, 2001).

Following the approach of Stern and Miyakoda (1995), we define the potential predictability (PP) of an index that varies depending on time (y) and on the ensemble dimension ($\eta$), as:

$$PP = \frac{\overline{X}_y}{\sigma_{iy}} \tag{1}$$

where $\overline{X}_y$ is the ensemble mean computed as

$$\overline{X}_y = \frac{1}{N}\sum_{\eta=1}^{N} X_{\eta y} \tag{2}$$

where N is the number of the members and y is the year. The denominator $\sigma_{iy}$ is the standard deviation among the members computed as

$$\sigma_{iy} = \frac{1}{N}\sum_{\eta=1}^{N}(X_{\eta y} - \overline{X_y})^2 \tag{3}$$

Hence PP is the ratio of the ensemble mean over the standard deviation among the members and a black bin in fig. 5 represents it for each year and for each index. According to the definition, the larger the value, the larger the potential predictability of that year. We can identify as largest values those in the tails (i.e. exceeding the 10th and 90th percentile) of the PP distribution (yellow bins in fig. 5). Typically the value of PP is large when the spread among the members is small (i.e. when the internal variability component is smaller than the forced one). In fig. 5 the ensemble spread is shown as well (black stars) and when PP is large the members values are close each other indicating their small standard deviation.

In fig. 5 (bottom right in each panel) we have reported also the ratio of the standard deviation of the ensemble mean over the average of the standard deviation for each member, which is as well a measure of the potential predictability of the indices (Alessandri et al., 2011). The intensity close to one indicate that the signal to noise ratio is high, and hence that their potential predictability is high. Large-scale monsoon indices have values larger than the local indices, and this may be related also to their dependence on less noisy fields like upper troposphere wind and geopotential height.

To identify the source of the forced potential predictability we can verify the correspondence between extreme monsoon predictable years and ENSO or IOD events. ENSO and IOD years (Table 1) have been classified using monthly SST anomalies based indices, i.e. NINO3 and IODM as previously defined. In particular, a year is classified as an ENSO-year when its NINO3 value exceeds 0.5 std from the mean (positive for El Niño and negative for La Niña) starting from November for at least 3 months (Trenberth, 1997). On the other hand, a year is classified as IOD when its IODM value averaged from September to November exceeds 1 std from the mean (positive for positive IOD event, and negative for a negative IOD event). For all the indices, we counted how many times extreme monsoon predictable years correspond to El Niño, La Niña or a positive or negative IOD event. The results are summarized in Table 2. For all the indices, at least half the time potentially predictable monsoon years coincide with an El Niño or a positive IOD event (see Table 2), actually in all the cases the two events co-occurred. On the other hand for negative IOD and La Niña events the correspondence is weaker (Table 2).

From fig. 5, 1987 can be identified as the year which has the largest potential predictability for all the indices: it corresponds to a positive IOD year co-occurring with a weak El Niño (Table 1). Actually, 1987 has been recorded as a drastic monsoon drought (Kumar, 1987). In the literature, 1987 and 1988 have been used as test beds to study the monsoon predictability as typical examples of a dry and a wet monsoon (Krishnamurti et al., 1995).

# 4 ISM characteristics during ENSO and IOD years

In this section most of the figures are types of Hoevmoeller diagrams, time-latitude or longitude-time plots. In all of them the monthly anomalies shown are composite of ENSO, IOD or extreme monsoon events computed over a three years period (hereafter 3-yrs composite). In particular, the time axis is organized over three years centered in the year (0), when the event peaks, and it covers the year before (-1) and the year after (+1) the peak, from spring to fall. Extreme monsoon years are classified as strong or weak depending on monsoon indices exceeding 1 or -1 standard deviation from the mean.

ENSO and IOD years (listed in Table 1) are the same for the observations/reanalysis and AMIP-type ensemble, as the classification is based on monthly SST anomalies and monthly SST is prescribed in those experiments. According to the metric used for the classification, years in Table 1 correspond to the November-December peak value for ENSO and to the fall peak value for the Indian Ocean Dipole (i.e. 1997 El Niño year refers to the event developing during 1997 and peaking between November 1997 and December 1998, while 1997 positive IOD year refers to the event peaking in September-November 1997).

## 4.1 Analysis of El Niño and La Niña years

Fig. 6 shows the 3yrs-composite of precipitation anomalies averaged over India (i.e. 75-85E) and of zonal wind shear anomalies averaged between 60E and 90E during El Niño and La Niña years (bold values in Table 1). In this case the year 0 corresponds to the developing phase of ENSO peaking from Nov(0) to Jan(+1), and with this methodology the summer season of year 0 corresponds to the ENSO developing phase, while that of year (-1) and that of year (+1) precedes and follows, respectively, an ENSO event. The anomalies are computed with respect to the monthly mean climatology of the period 1948-2003 in AMIP-type ensemble and observations, and of the whole century (1901-2000) in the coupled model experiment.

During the monsoon season of year (0), weaker than normal precipitation occurs over India, mainly in its second part (Aug(0)-Sep(0)) with reduced vertical zonal wind shear (fig. 6a). Boschat et al. (2011) firstly evidenced this asymmetry between the beginning and ending phase of the monsoon. The monsoon of the year before the El Niño evolution has stronger than normal precipitation, while the year that follows has weaker than normal rainfall north of 15N in the beginning of the monsoon season and stronger than normal precipitation in the southern part of India toward the end of the season (fig. 6a). As expected, over India increased/decreased zonal wind shear anomalies occur in correspondence of excess/deficit of rainfall (fig. 6a).

In the AMIP-type ensemble, the response of the monsoon characteristic during the summer season in correspondence of the evolution of the El Niño (fig. 6c) and the associated changes in the Walker circulation (as shown later) are realistic but the lack of ocean-atmosphere interaction prevents the Indian Ocean dynamics contribution to the biennial periodicity (Meehl et al., 2003; Wu and Kirtman, 2004). In the coupled model the signal is weak and for both the years preceding and following the monsoon the anomalies over India are not coherent in space (fig. 6c).

During La Niña years, the anomalies are reversed with respect to El Niño years even if the characteristics of precipitation and wind fields are not exactly opposite. In fact, in summer during the developing phase of La Niña, stronger than normal precipitation anomalies occur over India with larger values in the demise phase of the monsoon season, associated with higher than normal zonal wind shear anomalies (fig. 6b): the monsoon tends to be delayed and weaker (stronger) during El Niño (La Niña) years. The summer preceding La Niña has weaker than normal precipitation, in agreement with the reverse of the El Niño case. On the other hand, the summer following the peak of La Niña event has precipitation still stronger than normal, at least in the starting phase of the monsoon, different from the El Niño case (fig. 6b).

In the model, during La Niña years precipitation anomalies are largely weaker than observed both in the AMIP-type ensemble and in the coupled model experiment (fig. 6d,f). In the AMIP-type ensemble, the intensification of the wind shear in summer is realistic in intensity and time evolution during the monsoon season (fig. 6d). In the coupled model, in the summer of year 0 the signal of a more intense monsoon in terms of wind shear is mainly concentrated in the late monsoon season (fig. 6f).

The comparison between forced and coupled model experiments performances in fig. 6 reveals that AMIP-type simulations are more proxy to observations than the 20th century experiment is, and this is mostly true for the El Niño years. This difference could be ascribed to the weakness of the ENSO-monsoon connection in the coupled model used (see also Cherchi et al., 2007). This shortcoming of the model could be related to its biases, as documented by Gualdi et al. (2003) and Guilyardi et al. (2003), in the simulation of the basic state of the Pacific Ocean, like the common westward extension of the SST anomalies (Terray et al., 2005). These biases in fact could effect the location of subsidence in the Western Pacific and Indian Ocean sector (Cherchi et al., 2012).

### 4.2 Strong and weak monsoon years: Differences between indices

The ENSO-monsoon connection is interpreted in terms of the modulation of the Walker circulation, that can be represented with 200 mb velocity potential. Fig. 7 shows the composite for SST and 200 mb velocity potential during strong and weak monsoon years. The composites are built as described before, but the graphs are longitude versus time as the fields are averaged between 10S-10N. The region is chosen as it corresponds to the maxima in the evolution of the Walker cell (Lau and Yang, 2002). Here strong and weak monsoon years are classified based on IMI index. In the model, both for AMIP-type ensemble and for the coupled model experiment, the patterns shown for IMI do not differ from the same analysis applied to IMR and MTG indices (not shown), while in the reanalysis the conclusions may be different (which will be further discussed after the model outputs analysis). In the AMIP-type ensemble the indices are highly correlated each other, but we cannot exclude that this lack of variance in the model may be also influenced by biases in the coupling between rainfall and large-scale dynamics.

In the coupled model, negative (positive) 200 mb velocity potential anomalies over India peaking in summer are associated with upper troposphere divergence (convergence) and increased (decreased) low-level convergence over the region (fig. 7c,d): the patterns are almost symmetric comparing strong and weak monsoon years. The SST pattern has positive (negative) anomalies in the Pacific region during the summer monsoon season and in the months before. In the eastern part of the Indian Ocean weak positive (negative) anomalies develop after July (fig. 7c,d) in strong (weak) monsoon years. This pattern represents the enhanced dipole structure of the Indian Ocean in this model (Cherchi et al., 2007).

In the AMIP-type ensemble the characteristics are comparable with the coupled model experiment except that both SST and 200 mb velocity potential anomalies are larger during the summer monsoon season of year 0 (fig. 7a,b). In the AMIP-type ensemble the monsoon intensity is directly related with the simultaneous SST in the Pacific Ocean that modulates the dichotomy of subsidence regions between the Asian and the Pacific sectors. On the other hand, in the coupled model experiment the SST anomalies of the preceding season may change the atmospheric circulation patterns interacting with the anomalies in the Asian sector for strong monsoon years.

In the reanalysis the composite of IMI, IMR and MTG varies, suggesting different mechanisms at work in providing extreme monsoon rainfall and winds over India. Fig. 8 shows SST and 200 mb velocity potential composite for strong and weak monsoon years classified using IMI, IMR and MTG monsoon indices. In all the cases, the summer of year 0 is characterized by upper troposphere divergence (convergence) over the Indian Ocean sector in correspondence of stronger (weaker) than normal monsoon (fig. 8), but differences exist in the SST pattern potentially forcing (interacting with) those atmospheric anomalies.

IMI and IMR composites seem to represent two different conditions in terms of contemporary or precursor Pacific Ocean SST patterns influence. In fact, in IMR cases, starting from the spring of year 0, positive (negative) SST anomalies develop in the remote central-eastern Pacific sector and positive (negative) velocity potential anomalies in the upper troposphere peak over India thus providing weaker (stronger) than normal monsoon conditions (fig. 8c,d). On the other hand, in IMI cases negative (positive) SST anomalies in the Pacific sector in the winter before the peak (i.e. Oct(-1)-Jan(0)) precedes the development of positive (negative) 200 mb velocity potential anomalies typical of deficit (excess) rainfall conditions over India (fig. 8a,b).

In MTG cases the SST anomalies in the Pacific sector are larger than in the other cases and they are associated with anomalies of the same sign in the Indian Ocean developing in correspondence of the evolution of the monsoon season (fig. 8e,f). This figure shows how different condition in the Indian-Pacific sector may provide similar patterns over India. This result reflects the complexity of the relationship between ENSO, the monsoon and the Indian Ocean SST.

The list of the years used for the composites shown in fig. 8 are reported in Table 3.

For each index, the years corresponding to effective floods or droughts Indian monsoon events, according to the Indian Institute of Tropical Meteorology (IITM) classification (see www.tropmet.res.in/∼kolli/mol/Monsoon/Historical/air.html), are evidenced. For IMI and IMR, most of the events are effective extremes monsoon years, and even all the other matches with the sign of the ISM anomaly. On the other hand, the number of events in the MTG composite are fewer than in the other cases and few of them correspond to effective flood or drought years. If we restrict the analysis considering only the events that correspond with effective drought and flood monsoons, the main features just described are unchanged, even the SST pattern in the Indian sector (not shown).

### 4.3 Comparison between ENSO and IOD cases

To compare ISM characteristics during ENSO and IOD years, precipitation and zonal wind shear composites are computed also for positive and negative IOD events (fig. 9). In this case the year 0 corresponds to both the developing and peaking phase of IOD from Jul(0) to Nov(0). In the reanalysis a positive (negative) IOD peak is preceded by weaker (stronger) than normal monsoon rainfall and weaker (more intense) zonal wind shear (fig. 9a,b), even though the signals are small. In the positive IOD case Jun(0)-Jul(0) negative anomalies are followed by positive anomalies in rainfall mainly in Aug(0)-Sep(0) north of 20N (fig. 9a). In the negative IOD cases, the positive precipitation anomalies are particularly small and hardly identifiable. In the coupled model, the anomalies are weak and not coherent in space (fig. 9e,f), as for the ENSO case. In the AMIP-type ensemble, the anomalies during the summer monsoon period are large and extend for the whole monsoon season (fig. 9c,d).

To relate the results discussed above with the evolution of ENSO and IOD events, we have repeated SST and 200 mb velocity potential composite analysis for El Niño/La Niña and positive/negative IOD years (fig. 10 and fig. 11, respectively). In this case results from reanalysis and coupled model experiment are shown. In the Pacific basin positive (negative) SST anomalies develop from spring of year 0 to the summer of year +1 and they are preceded by anomalies of the opposite sign, but weaker, in the spring-summer of year -1 during El Niño (La Niña) events (fig. 10a,b). Over the Indian Ocean a dipole structure develops in correspondence of the El Niño years from July and it peaks in fall (fig. 10a). During La Niña years, the dipole signature in the Indian Ocean is weaker than during El Niño, and the negative anomalies in the western part of the basin are larger than the positive one in the east (fig. 10b).

During positive IOD events positive and negative SSTA in the western and eastern side of the Indian Ocean, respectively, are associated with positive SSTA in the Pacific Ocean in the contemporary season from April (0) to April (+1) (fig. 10c). In negative IOD cases, SSTA in both Indian and Pacific sectors are of the opposite sign but weaker in intensity: from this composite it seems that the IOD signal is dominated by the anomalies in the western part of the basin (fig. 10d). In the upper troposphere, the peak of the anomalies occur from spring to spring with negative anomalies in the Pacific sector and positive ones over the Indian region, corresponding to ENSO characteristics and explaining weakening of convergence. The anomalies are opposite during La Niña (fig. 10).

In the coupled model the SSTA and their time evolution in the Pacific Ocean are realistic and comparable with the observations, but the dipole signature in the Indian Ocean is stronger than observed, at least in the El Niño case, and it starts from spring (fig. 11a). During IOD years in the coupled model the anomalies are exactly symmetric with positive (negative) dipole anomalies in the Indian Ocean and positive (negative) SSTA in the Pacific sector developing from Jul (-1) and expanding westward (fig. 11c,d). In the model the IOD signal is large as this coupled model is particularly sensitive to the precipitation/wind feedback in the eastern part of the Indian Ocean (Gualdi et al., 2003; Cherchi et al., 2007). Differently from the observations, during positive (negative) IOD events dipole anomalies in the Indian Ocean are preceded by positive (negative) SSTA in the Pacific sector propagating from the year before (fig. 11c,d).

In recent decades El Niño and positive IOD events co-occurred in most of the cases (Ashok et al., 2001). In particular of ten positive IOD events classified in Table 1, five of them are also El Niño years (eight if we consider a 0.5 std threshold for the El Niño year classification). On the other hand, only one negative IOD co-occurred with La Niña events (they would be three if considering a weaker threshold for La Niña years classification) and most of them occurred before the 80s (Table 1). In the coupled model experiment, a similar behavior is found with half of the positive IOD events occurring in correspondence of El Niño years, and a few (two over eleven in a century) negative IOD events occurring during La Niña years. To distinguish the monsoon characteristics during El Niño and during positive IOD years we tried to separate the events as pure IOD (both positive and negative), pure ENSO (both El Niño and La Niña) and as co-occurring (positive IOD with El Niño and negative IOD with La Niña) events. Table 4 summarizes the results of the above classification with the list of the years as resulting from the HadISST dataset, and with the number of the events considered in the model. In some cases the number of the events selected is quite small (i.e. pure El Niño, or co-occurring negative IOD and La Niña events), hence we decided to focus on those cases with a sample robust enough to draw some conclusions. According to that, 3-years composite of SST and 200 mb velocity potential anomalies for pure positive and pure negative IOD, co-occurring positive IOD and El Niño and pure La Niña events are shown in fig. 12 for HadISST and NCEP collections and for the coupled model results.

During positive and negative IOD events, SST and 200 mb velocity potential anomalies are almost symmetric in both re-analysis and model. In fact, positive (negative) upper tropospheric velocity potential anomalies occur in summer-fall of year 0 over the Indian sector during positive (negative) IOD events and they correspond to weak (strong) monsoon characteristics (fig. 12a,c,e,g). In these cases, the main difference between the re-analysis and the coupled model is in the Pacific sector. In fact in the reanalysis the SSTA change from negative in spring-summer of year (-1) to positive in summer-fall of year (0) to negative again during spring-summer of year (+1) for positive IOD events, and the reverse occurs for negative IOD events (fig. 12a,c). On the other hand, in the model the SSTA in the Pacific sector oscillates from positive from Apr(-1) to Jul (0) to negative from Apr(+1) onwards during positive IOD events, and the reverse occurs during negative IOD events (fig. 12e,g). When positive IOD events and El Niño co-occur SST in the Pacific-Indian oceans sector and upper tropospheric velocity potential anomalies over India are larger than in pure cases in both re-analysis and coupled model experiment (fig. 12b,f). As previously mentioned, the model tends to overestimate the negative SSTA in the eastern side of the Indian Ocean (fig. 12f).

## 5 Changes in the ENSO-monsoon connection

Fig. 13 shows the correlations between ENSO, IOD and monsoon rainfall considering a 19 years sliding window in the data collections. The x-axis in the figure refers to the starting year of the 19 years correlation window. The dotted line corresponds to the correlation coefficients between NINO3 and IMR, so it represents the ENSO-monsoon connection. According to the figure since the beginning of the reanalysis record the relationship between ENSO and the monsoon is strong and negative, but since the middle of the 70s decade it starts to weakens up to becoming non-significant during the 90s and onwards.

A definite explanation for the changes occurring to the ENSO-monsoon connection has not been identified yet. Among possible explanations, changes in ENSO itself (Kumar et al., 2006), the global warming (Ashrit et al., 2001), the larger occurrence of IOD events (Ashok et al., 2004a) have been investigated. In fig. 13 the correlation coefficients between NINO3 and IODM (solid line) and between IODM and IMR (dashed line) are plotted as well to investigate more the role of the IOD in the changes occurring to the ENSO-monsoon relationship. The correlation between ENSO and IOD is strong positive and significant since the beginning of the time record considered, but it seems to be larger after mid 60s. However, changes in the intensity of the dotted and solid lines in fig. 13 are not evidently linked. That is, the ENSO-IODM correlation can be high both when the ENSO-monsoon connection is strong and significant and when it is weak and non-significant (i.e. after mid-80s). At the same time, the IOD-monsoon correlation shows multidecadal variability: it is negative and significant between mid 60s and mid 70s, while it is non-significant for the other periods. Decadal IOD signals, related with sub-surface ocean dynamics, have been investigated comparing oceanic reanalysis and coupled model experiments, where they appeared as a decadal modulation of interannual IOD events (Ashok et al., 2004b).

Fig. 13 provides a picture with periods having completely different characteristics in terms of mutual correlation intensities between ENSO, IOD and ISM in the reanalysis. In particular, in the first part of the record the ENSO-monsoon connection is strong, while the IOD-monsoon connection is non-significant and the IOD-ENSO correlation shows a change from non-significant to positive values. Then in the middle of the time record, the IOD-ENSO correlation intensifies and the monsoon-IOD correlation becomes negative and significant. In this framework, the ENSO-monsoon connection remains strong negative and significant. Finally toward the end of the record while the ENSO-IOD relationship remains strong, the others two start to decrease up to becoming non-significant. This result evidences how the mutual relationships are strictly connected but with a quite complex behavior. For example, the change around mid-70s of the IOD-monsoon relationship could correspond or be related with the weakening of the ENSO-monsoon connection, or both could be related to the changes occurring to ENSO itself (Kumar et al., 2006).

Before analyzing more the three periods identified we open a parenthesis on the model performance. As previously discussed, the coupled model has a weak ENSO-monsoon correlation. On the other hand, the correlations between IODM and IMR, and between NINO3 and IODM are large. In particular, the large IOD-monsoon relationship in summer could negatively influence the ENSO-monsoon connection as found also for the NCEP forecast model (Achuthavarier et al., 2012). Applying a 19-years sliding window to the correlation in the coupled model indices, it is not possible to identify drastic or periodic changes in the connection (not shown). Coupled models generally have difficulties in having this sort of changes or in general they are not able to reproduce climate shifts (i.e. Guilyardi, 2006, for ENSO).

The AMIP-type ensemble results have biases as well but the distinction between the correlations computed from the ensemble mean or as average of the members correlation gives some interesting outcomes. Fig. 14 shows the 19-years sliding correlation between ENSO and the monsoon (in the upper panel) and between the IOD and the monsoon (in the lower panel). In particular, the correlation coefficients between NINO3 and IMR are negative and significant up to mid'70s considering the ensemble mean (fig. 14a). On the other hand the average of the 9 members sliding correlation is almost never significant (fig. 14a). This result is consistent with the idea that the changes in the ENSO-monsoon connection depend on the changes occurred to ENSO itself, as in the AMIP-type ensemble mean the main contribution comes from the SST forcing, while the mean of the member correlation should contain the signal from the internal variability. The changes occurring to ENSO may be related to the different position of the SSTA peak of ENSO events in recent decades, as it has been recently discussed (Kumar et al., 2006).

Considering the correlation between IODM and IMR, the average of the 9 members correlations is never significant (fig. 14b, dashed line), while the correlation of the ensemble mean is negative and significant (as in the observations) in the first part of the record but not in the second one (fig. 14b, solid line). In this case, model and observations correspond for short periods with starting years between 1960 and 1965. While in the observations it is possible to identify a sort of decadal signal, in the AMIP-type ensemble mean there are sort of unrealistic shifts around 1960 and 1980. In this case the role of the SST forcing is not dominant as in the ENSO-monsoon, but there is also an important contribution from the internal variability component. We may speculate that the disagreement between model and observations is mostly related with the inability of this kind of experiments to have a realistic internal variability, as they miss the ocean-atmosphere coupling that is known to be crucial for Indian Ocean dynamics (Wu and Kirtman, 2004).

As mentioned before, considering the lines in fig. 13 and their interaction with the significance threshold we choose three sub-periods to perform some more analysis in terms of changes in ENSO-monsoon and IOD-monsoon relationship and their seasonal evolution in the reanalysis. The three periods are: 1949-1969 where the ENSO-monsoon connection is strong, while the IOD-monsoon connection is non-significant; 1962-1982 where both the connection are strong and 1980-2000 where the ENSO-monsoon connection is weak and the IOD-monsoon connection is non-significant.

Fig. 15 shows the time regression of the Indian summer monsoon rainfall index (IMR) on SST and 200 mb velocity potential for three different seasons: spring (AMJ mean) before the monsoon peak, summer (JAS mean) in correspondence of the monsoon peak and fall (OND mean) just after the monsoon peak. In summer, the Indian and Pacific sectors are characterized by opposite velocity potential anomalies in the upper troposphere with negative values in the former and positive values in the latter, in agreement with the typical ENSO teleconnection pattern (fig. 15b,e,h). In terms of SST, in the second period positive (negative) anomalies appear in the eastern (western) Indian basin, differently from the other two periods. In agreement with a stronger monsoon-IOD relationship, in this period larger negative SST anomalies are found in the northern Indian basin (both in the Arabian Sea and in the Bay of Bengal) because of the interaction between the basin and the monsoon rainfall (Cherchi et al., 2007).

However, the main differences between the three periods are found in the North Pacific and in the Atlantic sectors. In particular, in the last period when the ENSO-monsoon connection weakens, strong positive anomalies are found in the western Atlantic sector around 30N, with slight negative anomalies in the subtropical sector (Goswami et al., 2006; Kucharski et al., 2008), and in the western North Pacific (fig. 15h). On the other hand, before the 70s the positive anomalies in the North Pacific were mainly localized in the centre of the basin (fig. 15b). This difference may be related with the changes occurred in the North Pacific after 1976 (Miller et al., 1994) and to the associated differences in the ENSO teleconnections (Deser and Blackmon, 1995). This analysis cannot be considered exhaustive, but it highlights interesting issues in the ENSO-monsoon-IOD relationship on timescales with lower than interannual frequencies, which is worth of further studies.

## 6 Conclusions

Major portion of the Indian summer monsoon (ISM) variability is related to the variability in the Indian-Pacific sector. In this study, ISM variability has been investigated focusing on the monsoon characteristics in correspondence of ENSO and IOD events. The analysis has been performed comparing re-analysis and data with atmospheric (AMIP-type with forced interannually varying SST) and coupled model experiments.

ISM variability has been expressed here in terms of precipitation and circulation-based indices. In particular, large-scale monsoon indices, like DMI and MTG based on zonal wind shear and mid-tropospheric thickness, respectively, have been compared with local indices, like IMI and IMR based on low-level zonal wind and precipitation, respectively. Both model outputs and reanalysis, realistically represent the precipitation pattern variation in summer over India. In the AMIP-type ensemble the inter-annual variability of all the indices is significantly correlated with the reanalysis in terms of the ensemble mean, indicating that the forced SST component is important.

Using the AMIP-type ensemble we define and compute the potential predictability of the monsoon indices as the ratio of the ensemble mean over the standard deviation among the members for each monsoon index and for each year: the larger the value, the larger the potential predictability for that year. Strong and weak monsoon characteristics have comparable predictability in terms of large-scale and local monsoon indices. In the sample analyzed, about half of the more predictable extreme monsoon years coincide with an El Niño co-occurring with a positive IOD event. The result is consistent for all the indices.

Because of the seasonal evolution of the events, the monsoon in summer may be negatively influenced by the developing phase of ENSO, which peaks in the following winter and which may interact and influence the IOD anomalies in the subsequent fall. The 3-years composite analysis of precipitation and seasonal wind shear during ENSO and IOD events reveals that during El Niño and positive IOD years monsoon precipitation is reduced with weakened wind shear, while during La Niña and negative IOD events the monsoon characteristics are opposite with larger than normal rainfall and enhanced zonal wind shear. Actually, the ISM characteristics in El Niño/La Niña years or in positive/negative IOD events are not exactly symmetric. In fact, while during La Niña and negative IOD year the monsoon anomalies are almost uniform within the summer season, in the opposite cases (El Niño and positive IOD) there is a dipole in the anomalies within the season (i.e. anomalies in the demise phase of the monsoon change sign).

In the model composites, precipitation and wind shear anomalies are weaker than observed, mainly in the IOD cases. During ENSO events, AMIP-type ensemble results are more proxy to observations than the coupled model simulation is, and this could be also related to the weak ENSO-monsoon connection in this coupled model. In the AMIP-type ensemble the monsoon intensity is directly influenced by the simultaneous SST in the Pacific Ocean and its biennial characteristics are not captured because the lack of air-sea interactions in the Indian Ocean.

The composites of SST and 200 mb velocity potential during strong and weak monsoon years classified based on different monsoon indices highlight how different SST conditions in the Indo-Pacific sector may provide similar monsoon characteristics over India, reflecting the complexity of the relationship between ENSO, Indian Ocean SST and the monsoon.

In the reanalysis as well as in the coupled model most of the positive IOD events co-occurred with an El Niño, while that is not the case for La Niña. A further classification has been performed to separate years with pure IOD or ENSO events from years with co-occurring ENSO and IOD. Because of the number of cases involved, pure El Niño years as well as La Niña and negative IOD co-occurring events have not been taken into account. When positive IOD and El Niño co-occur the SST anomalies in the Indo-Pacific sector and 200 mb velocity potential anomalies over India are larger than in the pure cases. However, the model tends to overestimate the signal in the Indian Ocean, mainly in its eastern part.

The relationship between ENSO, IOD and the monsoon is not constant in time. In fact, in the record analyzed (i.e. 1948-2003) it is possible to distinguish periods with strong ENSO-monsoon connection, lack of IOD-monsoon connection and increasing ENSO-IOD relationship, or with both strong and negative IOD-monsoon and ENSO-monsoon connections, or with not-significant monsoon-ENSO and monsoon-IOD but with a strong ENSO-IOD relationships. The main difference between the periods identified is in the SST pattern of North Pacific and Atlantic sectors. When the ENSO-monsoon connection weakens, strong positive SST-IMR correlation is found in the western north Atlantic and north Pacific Ocean, the latter probably associated with the decadal changes of the North Pacific sector and the associated ENSO teleconnection. In the model it is not possible to identify those types of decadal changes. However, results from the AMIP-type ensemble suggest that while in the ENSO-monsoon case most of the correlation is driven by changes in the remote SST (and hence is somehow captured by the model), in the IOD-monsoon case changes in the correlation are not captured by the model, suggesting a predominance of its internal variability component and local model biases may influence as well its performance.

The study is quite heterogeneous in its analysis, but its main focus remains the analysis of the characteristics of the monsoon associated with ENSO and the IOD, spanning from composite analysis of specific classified events to the investigation of long timescales. The wide litterature on the differences in the characteristics of ENSO during the last decades (Wang, 1995; Ashok et al., 2007; McPhaden and Zhang, 2009; Jung et al., 2011, among others) may question whether factors like the intensity of the anomalies, the position of the SST maxima and the dynamics related to the SST development may have different impacts on the monsoon intensity and variability. According to that and considering the IOD decadal changes (Ashok et al., 2004b; Yuan and Yin, 2008) as well, composite analysis on specific ENSO and/or IOD years is worth of future investigation. Even if the model has been found particularly weak in the analysis of the variability at lower than interannual frequency, the results from the reanalysis suggest an important influence on the monsoon from other oceanic sectors rather than from the Indian-Pacific alone.

*Acknowledgements.* We are grateful to the anonymous reviewers whose comments help to improve the manuscript. We acknowledge the EU FP7-INCO INDO-MARECLIM project for financial support. The support of Italian Ministry of Education, University and Research, and Ministry for Environment, Land and Sea through the project GEMINA is gratefully acknowledged as well. AC thanks Dr A Alessandri for helpful comments on predictability issues.

## References


Achuthavarier D, Krishnamurthy V, Kirtman BP (2012) Role of the Indian Ocean in the ENSO-Indian summer monsoon teleconnection in the NCEP climate forecast system. J Clim 25: 2490–2508

Alessandri A, Borrelli A, Gualdi S, Scoccimarro E, Masina S (2011) Tropical Cyclone Count Forecasting Using a Dynamical Seasonal Prediction System: Sensitivity to Improved Ocean Initialization. J Clim 24: 2963–2982

Ashok K, Behera SK, Rao SA, Weng H, Yamagata T (2007) El Niño Modoki and its possible teleconnection. Geophys Res Lett 112 C11007

Ashok K, Guan Z, Saji NH, Yamagata T (2004a) Individual and combined influences of ENSO and the Indian Ocean Dipole on the Indian summer monsoon. J Clim 17: 3141–3155

Ashok K, Chan W-L, Motoi T, Yamagata T (2004b) Decadal variability of the Indian Ocean Dipole. Geophys Res Lett 31 L24207 doi: 10.1029/2004GL021345

Ashok K, Guan Z, Yamagata T (2001) Impact of the Indian Ocean Dipole on the relationship between the Indian monsoon rainfall and ENSO. Geophys Res Lett 28(23): 4499–4502

Ashrit RG, Rupa Kumar K, Krishna Kumar K (2001) ENSO-monsoon relationships in a greenhouse warming scenario. Geophys Res Lett 28: 1727–1730

Bellucci A, Gualdi S, Navarra A (2010) The Double-ITCZ Syndrome in Coupled General Circulation Models: The Role of Large-Scale Vertical Circulation Regimes. J Clim 23: 1127–1145

Boschat G, Terray P, Masson S (2011) Interannual relationships between Indian Summer Monsoon and Indo-Pacific coupled modes of variability during recent decades. Clim Dyn DOI:10.1007/s00382-010-0887-y

Bracco A, Kucharski F, Molteni F, Hazeleger W, Severijns C (2007) A recipe for simulating the interannual variability of the Asian summer monsoon and its relation with ENSO. Clim Dyn 28: 441–460

Charney JG, Shukla J (1981) Predictability of monsoons. In: Monsoon dynamics (Lighthill J, Pearce RP, eds). Cambridge: Cambridge University Press, pp 99–108

Cherchi A, Masina S, Navarra A (2012) Tropical Pacific-North Pacific teleconnection in a coupled GCM: remote and local effects. Int J Climatol 32: 1640–1653

Cherchi A, Masina S and Navarra A (2008) Impact of extreme $CO_2$ levels on tropical climate: A CGCM study. Clim Dyn 31: 743–758

Cherchi A, Gualdi S, Behera S, Luo JJ, Masson S, Yamagata T, Navarra A (2007) The influence of tropical Indian Ocean SST on the Indian summer monsoon. J Clim 20: 3083–3105

Cherchi A, Navarra A (2007) Sensitivity of the Asian summer monsoon to the horizontal resolution: differences between AMIP-type and coupled model experiments. Clim Dyn 28: 273–290

Deser C, Blackmon M (1995) On the relationship between tropical and North Pacific SST variations. J Clim 8: 1677–1680

Goswami BN (1994) Dynamic predictability of seasonal monsoon rainfall: Problems and prospects. Proc Indian Nat Acad Sci 60A: 101–120

Goswami BN (1998) Interannual variations of Indian summer monsoon in a GCM: External conditions versus internal feedbacks. J Clim 11: 501–521

Goswami BN, Xavier PK (2005) Dynamics of internal interannual variability of the Indian summer monsoon in a GCM. J Geophys Res 110 D24104

Goswami BN, Madhusoodanani MS, Neema CP, Sengupta D (2006) A physical mechanism for North Atlantic SST influence on the Indian summer monsoon. Geophys Res Lett 33(2) L02706

Gualdi S, E Scoccimarro and A Navarra (2008) Changes in Tropical Cyclone Activity due to Global Warming: Results from a High-Resolution Coupled General Circulation Model. J Climate 21 5204-5228

Gualdi S, Guilyardi E, Navarra A, Masina S, Delecluse P (2003) The interannual variability in the tropical Indian Ocean as simulated by a CGCM. Clim Dyn 20: 567–582

Guilyardi E, Delecluse P, Gualdi S, Navarra A (2003) Mechanisms for ENSO phase change in a coupled GCM. J Clim 16: 1141–1158

Guilyardi E (2006) El Niño-mean state-seasonal cycle interactions in a multi-model ensemble. Clim Dyn 26: 329–348

Izumo T, Vialard J, Lengaigne M, de Boyer Montegut C, Behera SK, Luo JJ, Cravatte S, Masson

S, Yamagata T (2010) Influence of the state of the Indian Ocean dipole on the following year's El Niño. Nature Geoscience, 3: 168–172

Ju J, Slingo J (1995) The Asian summer monsoon and ENSO. Quart J Roy Meteor Soc 121: 1133–1168

Jung C, An S-I, Kug J-S, Yeh SW (2011) The role of mean state on changes in El Niño flavor. Clim Dyn 37(5-6): 1205–1215

Kalnay E, Kanamitsu M, Kistler R, and co-authors (1996) The NCEP/NCAR 40-Year Reanalysis Project. Bull Am Meteor Soc 77: 437-471

Kang IS, Lee JY, Park C-k (2004) Potential predictability of summer mean precipitation in a dynamical seasonal prediction system with systematic error correction. J Clim 17: 834–844

Kawamura R (1998) A possible mechanism of the Asian summer monsoon-ENSO coupling. J Meteor Soc Japan 76: 1009–1027

Kinter III JL, Miyakoda K, Yang S (2002) Recent changes in the connection from the Asian monsoon to ENSO. J Clim 15: 1203–1215

Kirtman BP, Shukla J (2000) Influence of the Indian summer monsoon on ENSO. Quart J Roy Meteor Soc 126: 213–239

Krishnamurti TN, Bedi HS, Rohaly G, Fulakeza M, Oosterhof D, Ingles K (1995) Seasonal monsoon forecast for the years 1987 and 1988. Glob Planet Change 10: 79–95

Krishnamurthy V, Shukla J (2001) Observed and model simulated interannual variability of the Indian monsoon. Mausam 52: 133–150

Kucharski F, Bracco A, Yoo JH, Molteni F (2008) Atlantic forced component of the Indian monsoon interannual variability. Geophys Res Lett 35 L04706 doi: 10.1029/2007GL033037

Kumar A (1987) Consequences of the 1987 monsoon failure: A preliminary assessment. Econ Politic Weekly 22(39): 1635–1640

Kumar KK, Rajagopalan B, Hoerling M, Bates G, Cane M (2006) Unraveling the mystery of Indian Monsoon failure during El Niño. Science 314: 115–119.

Kumar, KK, Rajagopalan B, Kane MA (1999) On the weakening relationship between the Indian monsoon and ENSO. Science 284: 2156–2159

Lau KM, Yang S (2002) Walker circulation. In: *Encyclopedia of Atmospheric Sciences*. Eds. J Holton, JP Pyle, J Curry. Academic Press

Lau N-C, Wang B (2006) Interactions between the Asian monsoon and the El Niño Southern Oscillation. In: ”The Asian monsoon”, B. Wang Ed, Springer-Praxis, 479–511

Li T, Wang B, Chang CP, Zhang YS (2003) A theory for the Indian Ocean Dipole-Zonal Mode. J Atmos Sci 60: 2119–2135

Madec G, Delecluse P, Imbard M, Levy C (1998) OPA version 8.1 Ocean General Circulation Model reference manual. Technical report, LODYC/IPSL Note 11

McPhaden MJ, Zhang X (2009) Asymmetry in zonal phase propagation of ENSO sea surface temperature anomalies. Geophys Res Lett 36 L13703

Meehl GA (1994) Coupled land-ocean-atmosphere processes and South Asian monsoon variability. Science 266: 263–267

Meehl GA (1997) The South Asian monsoon and the tropospheric biennial oscillation. J Climate 10: 1921–1943

Meehl GA, Arblaster JM, Loschnigg J (2003) Coupled ocean-atmosphere dynamical processes in the Tropical Indian and Pacific Oceans and the TBO. J Clim 16: 2138–2158

Miller AJ, Cayan DR, Barnett TP, Graham NE, Oberhuber JM (1994) The 1976-77 climate shift for the Pacific Ocean. Oceanogr 7: 21–26

Mitchell TD, Jones PD (2005) An improved method of constructing a database of monthly climate observations and associated high-resolution grids. Int J Climatol 25 693–712

Mohan RSA, Goswami BN (2003) Potential predictability of the Asian summer monsoon on monthly and seasonal time scales. Meteor Atm Phys 84: 83–100

Parthasarathy B, Munot AA, Kothwale DR (1992) Indian summer monsoon rainfall indices: 1871–1990. Meteorol Mag 121: 174–186

Pokhrel S, Chaudhari HS, Saha SK, Dhakata A, Yadav RK, Salenke K, Mahaptra S, Rao SA (2012) ENSO, IOD and Indian summer monsoon in the NCEP climate forecast system. Clim Dyn DOI: 10.1007/s00382-012-1349-5

Rasmusson EM, Carpenter TH (1983) The relationship between eastern equatorial Pacific sea surface temperature and rainfall over India and Sri Lanka. Mon Wea Rev 111: 517–528

Rayner NA, Parker DE, Horton EB, Folland CK, Alexander LV, Rowell DP, Kent EC, Kaplan A (2003) Global analysis of sea surface temperature, sea ice and night marine air temperature since the late nineteenth century. J Geophys Res 18(D14) 4407 DOI:10.1029/2002JD002670

Roeckner E, Arpe K, Bengtsson L, Christoph M, Claussen M, Dümenil L, Esch M, Giorgetta M, Schlese U, Schulzweida U (1996) The Atmospheric general circulation Model ECHAM4: Model description and simulation of present-day climate. *Max-Planck Institut für Meteorologie*, Report no. 218, Hamburg, 86 pp

Rowell DP (1998) Assessing potential seasonal predictability with an ensemble of multidecadal GCM simulations. J Clim 11: 109–120

Saji NH, Yamagata T (2003) Possible impacts of Indian Ocean dipole mode events on global climate. Clim Res 25: 151–169

Saji NH, Goswami BN, Vinaychandran PN, Yamagata T (1999) A dipole mode in the Tropical Indian Ocean. Nature 401: 360-363

Shinoda T, Alexander MA, Hendon HH (2004) Remote response of the Indian Ocean to interannual SST variations in the Tropical Pacific. J Clim 17: 362–372

Shukla J (1981) Dynamical predictability of monthly means. J Atmos Sci 38: 2547–2572

Sikka DR (1980) Some aspects of the large-scale fluctuations of summer monsoon rainfall over India in relations to fluctuations in the planetary and regional scale circulation parameter. J Earth Sys Sci 89: 179–195

Singh SV, Kriplani RH (1986) Potential predictability of lower-tropospheric monsoon circulation and rainfall over India. Mon Wea Rev 114: 758–763

Sperber KR, Slingo J, Annamalai H (2000) Predictability and relationship between sub-seasonal and interannual variability during the Asian summer monsoons. Q J R Meteor Soc 126: 2545–2574

Stern W, Miyakoda K (1995) Feasibility of seasonal forecasts inferred from multiple GCM simulations. J Clim 8: 1071–1085

Tamura T, Koike T, Yamamoto A, Yasukawa A, Kitsuregawa M (2011) Contrasting impacts of the

Indian Ocean dipole and ENSO on the tropospheric biennial oscillation. SOLA 7: 13-16
Tanaka HL, Ishizaki N, Kitoh A (2004) Trend and interannual variability of Walker, monsoon and Hadley circulations defined by velocity potential in the upper troposphere. Tellus 56A: 250–269
Terray P, Guilyardi E, Fischer AS, Delecluse P (2005) Dynamics of the Indian monsoon and ENSO relationships in the SINTEX global coupled model. Clim Dyn 24: 145–168
Trenberth K (1997) The definition of El Niño. Bull Am Meteor Soc 78(12): 2771–2777
Turner AG, Annamalai H (2012) Climate change and the South Asian summer monsoon. Nature Clim Change 2: 1-9
Turner AG, Sperber KR, Slingo J, Meehl G, Mechoso CR, Kimoto M, Giannini A (2011) Modelling monsoons: understanding and predicting current and future behaviour. In: Chang CP, Ding Y, Lau NC, Johnson RH, Wang B, Yasunari T (Eds) ”The Global monsoon system: Research and forecast”, 2nd Ed, World Scientific Publishing Co, Singapore, pp 421–454
Turner AG, Inness PM, Slingo JM (2007) The effect of doubled CO2 and model basic state biases on the monsoon-ENSO system. I: Mean response and interannual variability. Quart J Roy Meteorol Soc 133: 1143–1157
van Oldenborgh GJ, Burgers G (2005) Searching for decadal variations in ENSO precipitation teleconnections. Geophys Res Lett 32 L15701
Walker GT (1924) Correlation in seasonal variations of weather, IX: A further study of world weather. Mem Ind Meteor Dept 24: 275–332
Wang B (1995) Interdecadal Changes in El Niño Onset in the Last Four Decades. J Clim 8: 267–285
Wang B, Wu R, Lau K-M (2001) Interannual variability of the Asian summer monsoon: Contrast between the Indian and the Western North Pacific-East Asian monsoons. J Clim 14: 4073–4090
Wang B, Fan Z (1999) Choice of South Asian summer monsoon indices. Bull Am Meteor Soc 80(4): 629–638
Webster P, Hoyos CD (2010) Beyond the spring barrier? Nature Geoscience 3: 152–153
Webster PJ, Magaña V, Palmer TN, Shukla J, Tomas RA, Yanai M, Yasunari T (1998) Monsoons: processes, predictability and the prospects for prediction. J Geophys Res 103: 14 451–14 510

Webster PJ, Moore AM, Loschnigg JP, Leben RR (1999) Coupled ocean-atmosphere dynamics in the Indian Ocean during 1997-1998. Nature 401: 356–360

Webster PJ, Clark C, Cherikova C, Fasullo J, Han W, Loschnigg J, Sahami K (2002) ”The monsoon as a self-regulating coupled ocean-atmosphere system”. Meteorology at the Millennium. Academic Press, 198–219

Webster PJ, Yang S (1992) Monsoon and ENSO: Selectively interactive systems. Quart J Roy Meteor Soc 118: 877–926

Wu R, Kirtman BP (2007) Role of the Indian Ocean in the biennial transition of the Indian summer monsoon. J Clim 20: 2147–2164

Wu R, Kirtman BP (2004) Impact of the Indian Ocean on the Indian summer monsoon-ENSO relationship. J Clim 17: 3037–3054

Xavier PK, Marzin C, Goswami BN (2007) An objective definition of the Indian summer monsoon season and a new perspective on the ENSOmonsoon relationship. Quart J Roy Meteor Soc 133: 749–764

Xie P, Arkin PA (1997) Global precipitation: A 17-year monthly analysis based on gauge observations, satellite estimates, and numerical model outputs. Bull Amer Meteor Soc 78: 2539–2558

Yuan Y, Yin LC (2008) Decadal variability of the IOD-ENSO relationship. Chin Sci Bull 53: 1745–1752

# Tables

| | List of years |
|---|---|
| El Niño | 1951 **1957**, 1963, **1965**, 1968, 1969, **1972**, 1976, 1977 **1982**, 1986, 1987, **1991**, **1994**, **1997**, 2002 |
| La Niña | **1949**, 1950, 1954, **1955**, 1956, 1964, 1967, **1970**, 1971, **1973**, **1975** **1984**, **1988**, 1995, 1998, **1999**, 2000 |
| positive IOD | 1961, 1963, 1967, 1972, 1982, 1987, 1991, 1994, 1997, 2002 |
| negative IOD | 1956, 1958, 1960, 1964, 1968, 1974, 1975, 1992, 1996, 1998 |

**Table 1.** List of El Niño, La Niña, positive and negative IOD years, based on the values of NINO3 and IODM indices, respectively. IOD years are computed from values averaged in SON exceeding 1 standard deviation from the mean, and they mostly agree with previous classifications (Saji and Yamagata, 2003; Yuan and Yin, 2008, among others). ENSO years are shown based on NDJ values (see text for more details) exceeding 0.5 std (years exceeding 1 std are in **bold**). All El Niño/La Niña years in the table agree with US National Weather Service classification (http://www.cdc.noaa.gov/products/analysis_monitoring/ensostuff/ensoyears.html).

| | pIOD | El Niño | nIOD | La Niña |
|---|---|---|---|---|
| IMR | 0.5 | 0.5 | 0.5 | 0.3 |
| IMI | 0.5 | 0.5 | 0.2 | 0.3 |
| DMI | 0.7 | 0.7 | 0.3 | 0.5 |
| MTG | 0.5 | 0.5 | 0.5 | 0.8 |

**Table 2.** Fraction of extreme monsoon predictable years (yellow bins from fig. 5) corresponding to a positive IOD event (pIOD), an El Niño event, a negative IOD (nIOD) event and a La Niña event (columns from left to right) for IMR, IMI, DMI and MTG monsoon indices (rows from top to bottom). El Niño/La Niña and positive/negative IOD years are listed in Table 1.

| Monsoon index | Strong mons yrs (¿1std) | Weak mons yrs (¡-1std) |
|---|---|---|
| IMI | 1958, **1959**, **1961**, **1970**, 1973<br>1975 1978, 1980, **1994** | 1949, 1950, 1962, **1965**, **1966**, **1972**<br>**1974**, **1979**, **1987**, 1999 |
| IMR | 1949, 1953, **1956**, **1959**, **1961**<br>1964, 1973, **1975**, 1978, **1988**, 1990 | 1952, 1957, 1965, 1966, 1968, 1972<br>1974, 1979, 1982, 1987, 1992, 2002 |
| MTG | 1948, 1954, 1961, 1967<br>1971, 1978, 1981, 1984, 1985 | 1957, 1969, 1972, 1983<br>1987, 1992, 1997, 2002 |

**Table 3.** List of years corresponding to strong and weak monsoon events according to IMI, IMR and MTG values larger than 1 standard deviation from the mean, or lower than -1 standard deviation from the mean, respectively. Years in **bold** correspond to floods and drought Indian summer monsoon events according to AIR (All-Indian Rainfall) index from IITM website (www.tropmet.res.in/∼kolli/mol/Monsoon/Historical/air.html).

| Type of event | List of years (HadISST) | # of years (SSXX) |
|---|---|---|
| pure pIOD | 1961, 1963, 1967, 1987, 2002 | 8 |
| pIOD/ElNino | 1972, 1982, 1991, 1994, 1997 | 8 |
| pure ElNino | 1957, 1965 | 3 |
| pure nIOD | 1956, 1958, 1960, 1964, 1968<br>1974, 1992, 1996, 1998 | 9 |
| nIOD/LaNina | 1975 | 2 |
| pure LaNina | 1949, 1955, 1970, 1973, 1984, 1988, 1999 | 12 |

**Table 4.** List of years (second column) from the HadISST and number of years (third column) considered in the coupled model experiment (SSXX), respectively, of the events classified (from top to bottom) as: pure positive IOD (pIOD), co-occurring positive IOD and El Niño (pIOD/ElNino), pure El Niño, pure negative IOD (nIOD), co-occurring negative IOD and La Niña (nIOD/La Niña) and pure La Niña.

## Figure Captions

**Fig. 1.** Annual cycle of precipitation (mm/d, shaded) and zonal wind shear (m/s, contours) zonally averaged between 60-90E for (a) CMAP and NCEP reanalysis, (b) AMIP-type ensemble mean and (c) coupled model experiment (SSXX). The zonal wind shear is computed as difference between lower and upper tropospheric zonal wind (U850 minus U200).

**Fig. 2.** JJA mean precipitation (mm/d, shaded) and 200 mb velocity potential ($\times\ 10^6$ 1/s$^2$, contours with the thicker black line in correspondence of zero values) for (a) CMAP and NCEP reanalysis, (b) the AMIP-type ensemble mean and (c) the coupled model experiment (SSXX) outputs. (d) JJA mean SST (°C) for the HadISST dataset (contours, with the 28°C isotherm identified by the thicker red line), and JJA mean SST difference between the coupled model experiment and the HadISST dataset (shaded).

**Fig. 3.** Lagged correlation between JJA IMR and NINO3 (solid line) and IODM (dashed line) monthly anomalies indices for (a) CRU and HadISST datasets and (b) AMIP-type ensemble. Horizontal lines in both panels correspond to the threshold values for the statistical significance at 90%.

**Fig. 4.** Annual cycle of monsoon indices, (a) IMR, (b) IMI, (c) DMI and (d) MTG, for CRU and NCEP data (black line), AMIP-type ensemble (blue line) and coupled model experiment (SSXX, green line).

**Fig. 5.** Potential predictability (PP) for the monsoon indices, (a) IMR, (b) IMI, (c) DMI and (d) MTG, in the AMIP-type ensemble. Yellow bin correspond to PP values in the tails (exceeding 10th and 90th percentiles) of the distribution. Black stars correspond to the index values for each member of the ensemble to evidence the ensemble spread. The value in the bottom right of each

panel is the ratio of the standard deviation of the ensemble mean and the average of the standard deviation of each member (see text for more details).

**Fig. 6.** 3-years composite of precipitation (mm/day, shaded) and zonal wind shear (m/s, contours) anomalies averaged over the Indian continent (75-85E) and in the region 60-90E, respectively. The values shown are computed as El Niño and La Niña composites for (a,b) CRU and NCEP datasets, (c,d) AMIP-type ensemble and (e,f) coupled model experiment (SSXX). In the model experiments, precipitation is masked over ocean to consider land-points only.

**Fig. 7.** 3-years composite of SST (°C, shaded) and 200 mb velocity potential ($\times$ 1.e+6 1/s$^2$, contours) anomalies averaged between 10S and 10N. The values shown are computed as strong and weak monsoon years composites for (a,b) AMIP-type ensemble and (c,d) coupled model experiment (SSXX). Strong/weak monsoon years are classified based on IMI index.

**Fig. 8.** Same as fig. 7, but strong and weak monsoon years are classified based on (a,b) IMI, (c,d) IMR and (e,f) MTG indices in the HadISST and NCEP datasets.

**Fig. 9.** Same as fig. 6, but the composites are computed for positive (left panels) and negative (right panels) IOD events.

**Fig. 10.** 3-years composite of SST (°C, shaded) and 200 mb velocity potential ($\times$ 1.e+6 1/s$^2$, contours) anomalies averaged between 10S and 10N. The values shown are (a,b) El Niño and La Niña composites and (c,d) positive and negative IOD composites for HadISST and NCEP datasets.

**Fig. 11.** Same as fig. 10, but for the coupled model experiment (SSXX).

**Fig. 12.** Same as fig. 10, but the values shown are composite of (a,e) pure positive IOD (pure pIOD), (b,f) combined positive IOD and El Niño (pIOD/ElNino), (c,g) pure negative IOD (pure

nIOD) and (d,h) pure La Niña (pure LaNina) events in the HadISST and NCEP datasets (upper panels) and in the coupled model experiment (SSXX, lower panels).

**Fig. 13.** 19 years sliding correlations between IODM and NINO3 (black solid line), IODM and IMR (dashed line), NINO3 and IMR (dotted line) from the CRU and HadISST datasets. Solid horizontal lines indicate the statistical significance threshold at 95%. Years in the x-axis correspond to the starting year of the 19 years correlation window.

**Fig. 14.** 19 years sliding correlations between (a) NINO3 and IMR and (b) IODM and IMR in the AMIP-type ensemble. In both panels, ensemble mean value (solid line) and the average of the correlation for each member of the ensemble (dashed line) are shown. The solid horizontal line corresponds to the statistical significance threshold at 95%. Years in the x-axis correspond to the starting year of the 19 years correlation window.

**Fig. 15.** Time-regression of Indian summer monsoon rainfall (IMR) on SST ($^\circ$C, shaded) and 200 mb velocity potential ($\times$ 1.e+6 $1/s^2$, contours) during spring (AMJ mean, upper panels), summer (JAS mean, middle panels) and fall (OND mean, lower panels) for (a,b,c) 1949-1969, (d,e,f) 1962-1982 and (g,h,i) 1980-2000 time periods.

# Figures

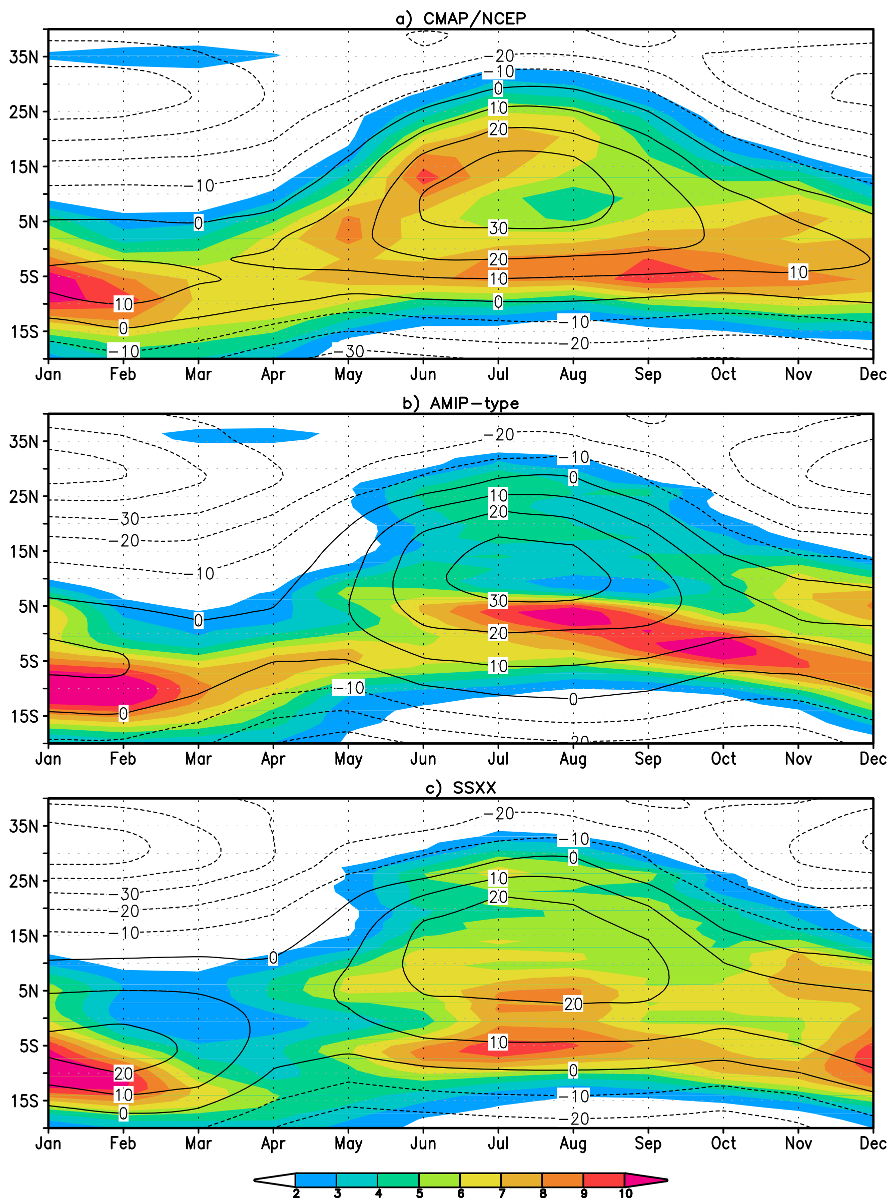


**Fig. 1.** Annual cycle of precipitation (mm/d, shaded) and zonal wind shear (m/s, contours) zonally averaged between 60-90E for (a) CMAP and NCEP reanalysis, (b) AMIP-type ensemble mean and (c) coupled model experiment (SSXX). The zonal wind shear is computed as difference between lower and upper tropospheric zonal wind (U850 minus U200).

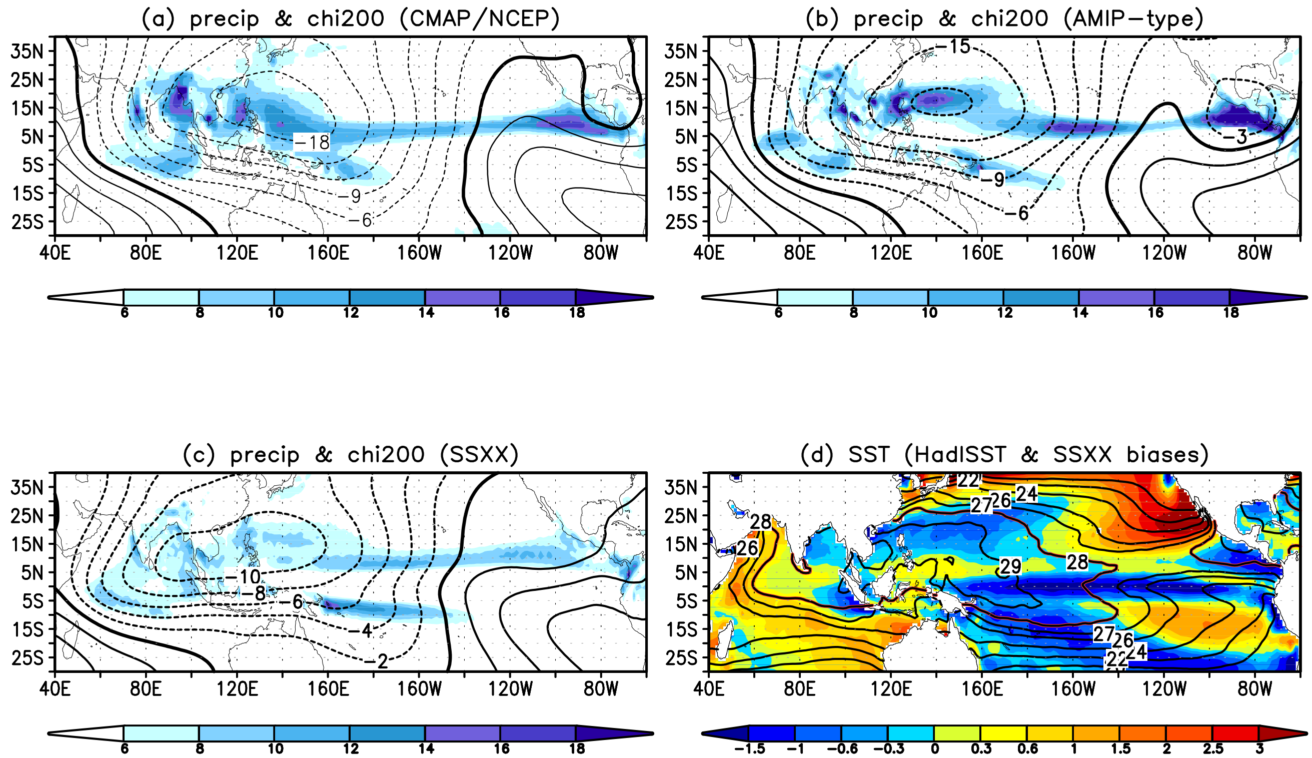


**Fig. 2.** JJA mean precipitation (mm/d, shaded) and 200 mb velocity potential ($\times\ 10^6$ 1/s$^2$, contours with the thicker black line in correspondence of zero values) for (a) CMAP and NCEP reanalysis, (b) the AMIP-type ensemble mean and (c) the coupled model experiment (SSXX) outputs. (d) JJA mean SST (°C) for the HadISST dataset (contours, with the 28°C isotherm identified by the thicker red line), and JJA mean SST difference between the coupled model experiment and the HadISST dataset (shaded).

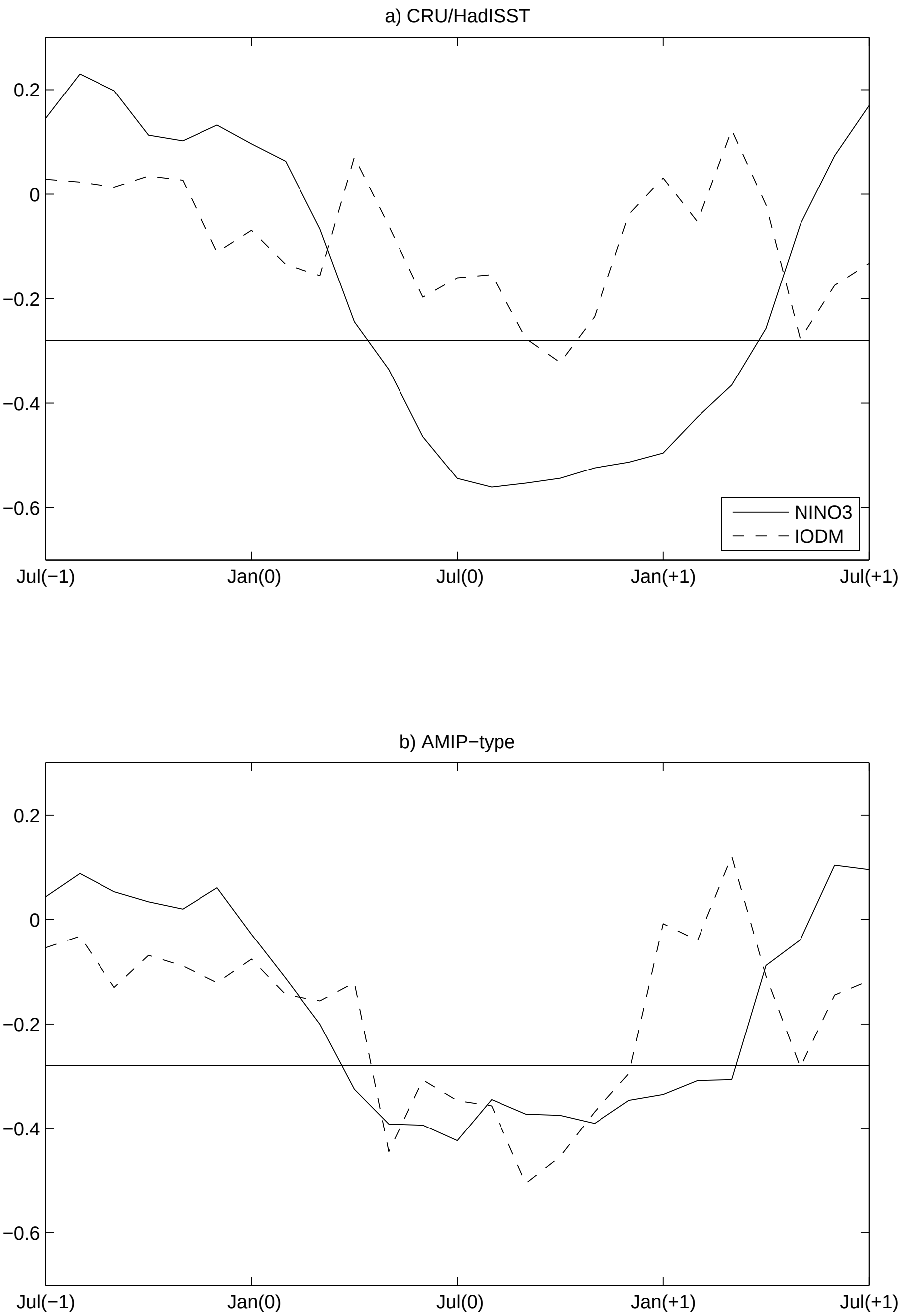


**Fig. 3.** Lagged correlation between JJA IMR and NINO3 (solid line) and IODM (dashed line) monthly anomalies indices for (a) CRU and HadISST datasets and (b) AMIP-type ensemble. Horizontal lines in both panels correspond to the threshold values for the statistical significance at 90%.

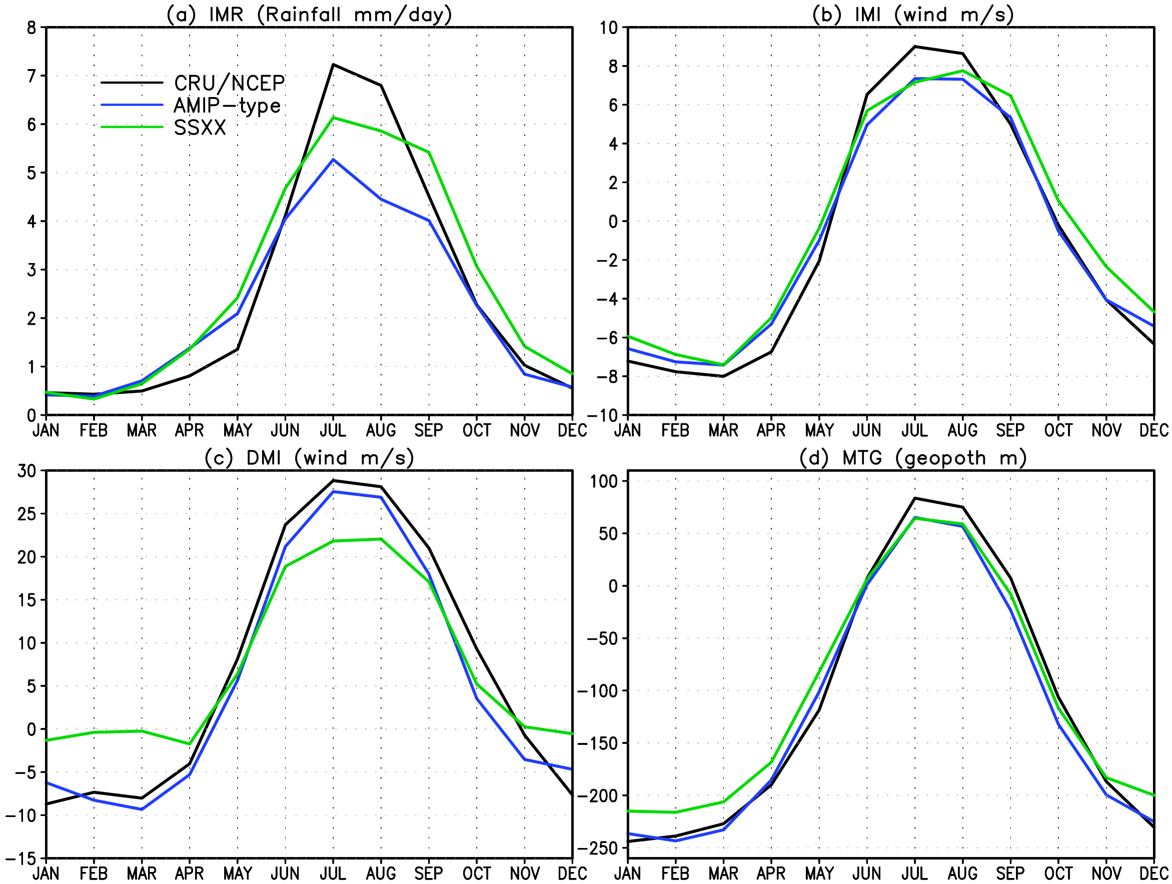


**Fig. 4.** Annual cycle of monsoon indices, (a) IMR, (b) IMI, (c) DMI and (d) MTG, for CRU and NCEP data (black line), AMIP-type ensemble (blue line) and coupled model experiment (SSXX, green line).

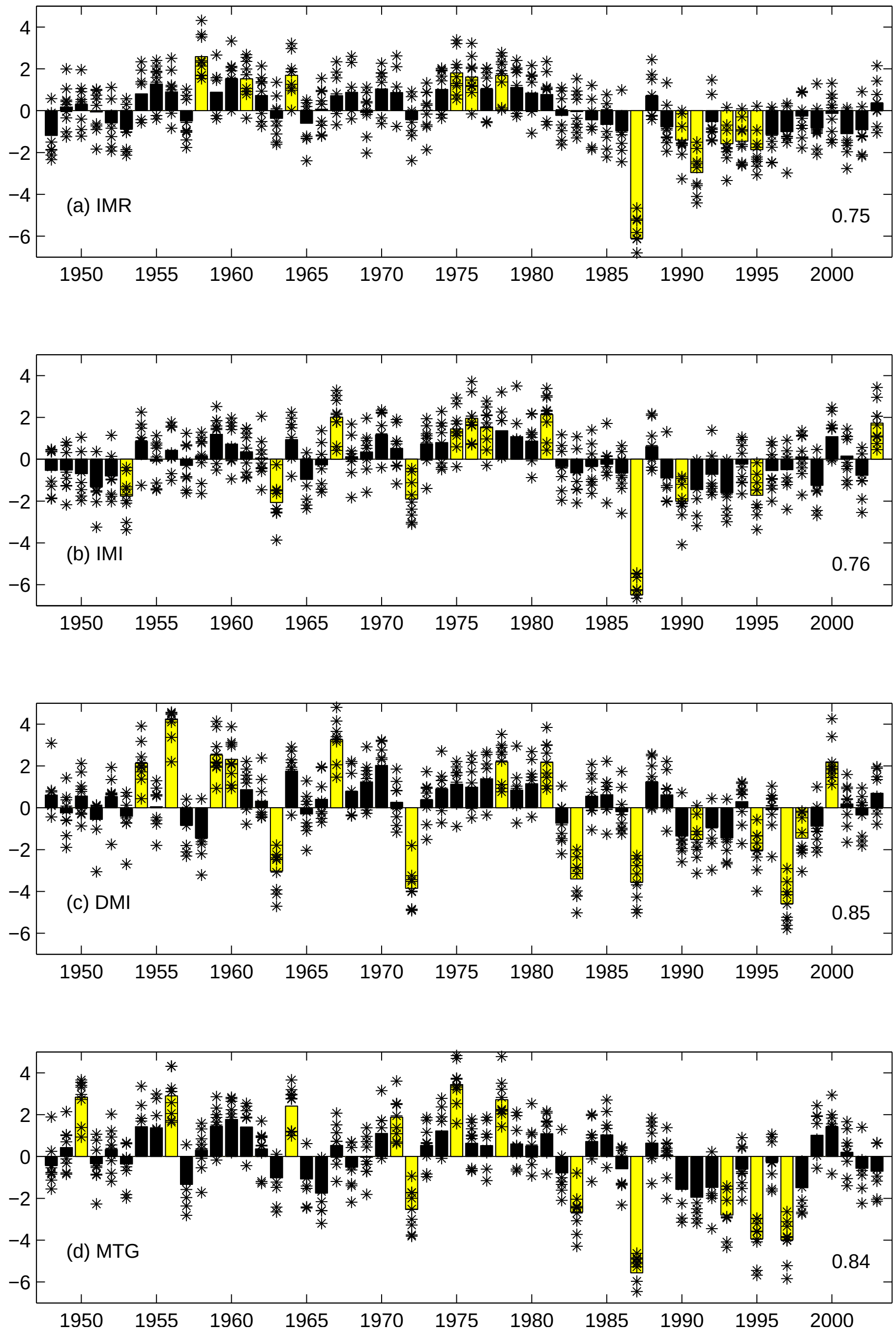


**Fig. 5.** Potential predictability (PP) for the monsoon indices, (a) IMR, (b) IMI, (c) DMI and (d) MTG, in the AMIP-type ensemble. Yellow bin correspond to PP values in the tails (exceeding 10th and 90th percentiles) of the distribution. Black stars correspond to the index values for each member of the ensemble to evidence the ensemble spread. The value in the bottom right of each panel is the ratio of the standard deviation of the ensemble mean and the average of the standard deviation of each member (see text for more details).

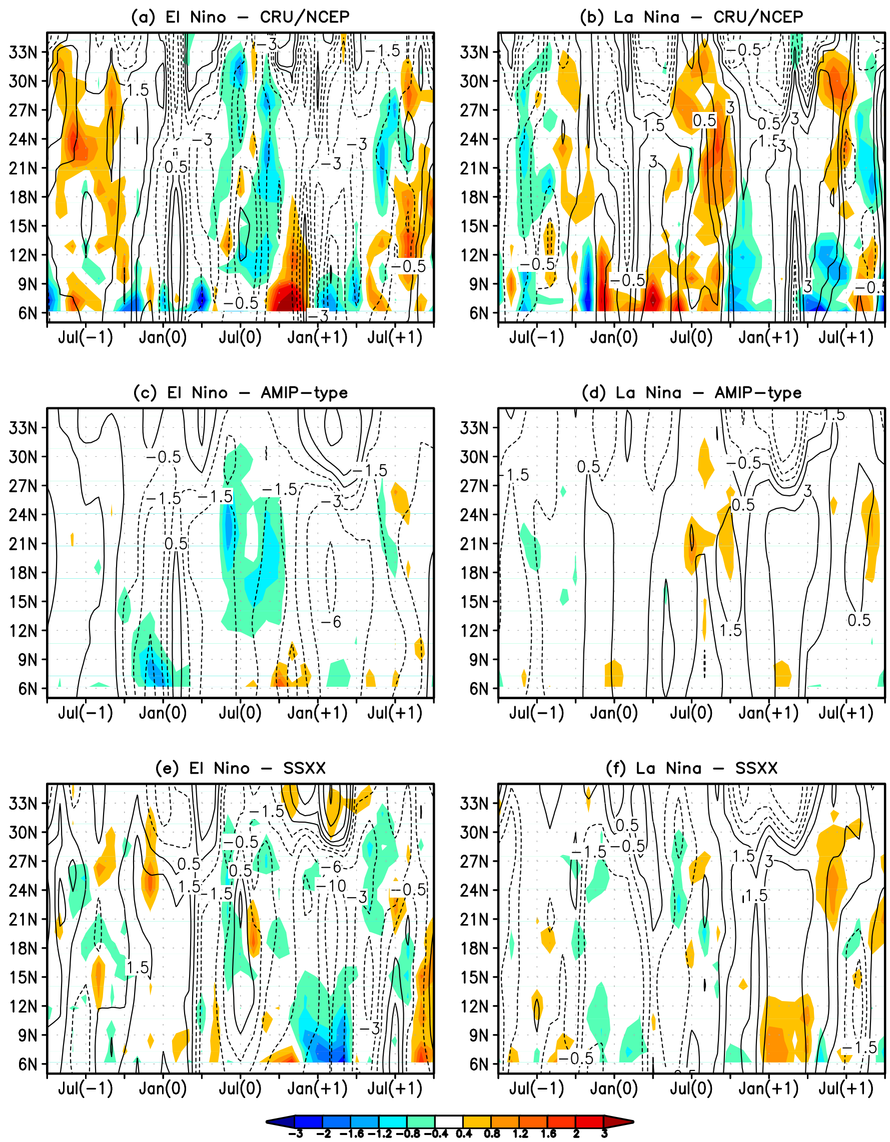


**Fig. 6.** 3-years composite of precipitation (mm/day, shaded) and zonal wind shear (m/s, contours) anomalies averaged over the Indian continent (75-85E) and in the region 60-90E, respectively. The values shown are computed as El Niño and La Niña composites for (a,b) CRU and NCEP datasets, (c,d) AMIP-type ensemble and (e,f) coupled model experiment (SSXX). In the model experiments, precipitation is masked over ocean to consider land-points only.

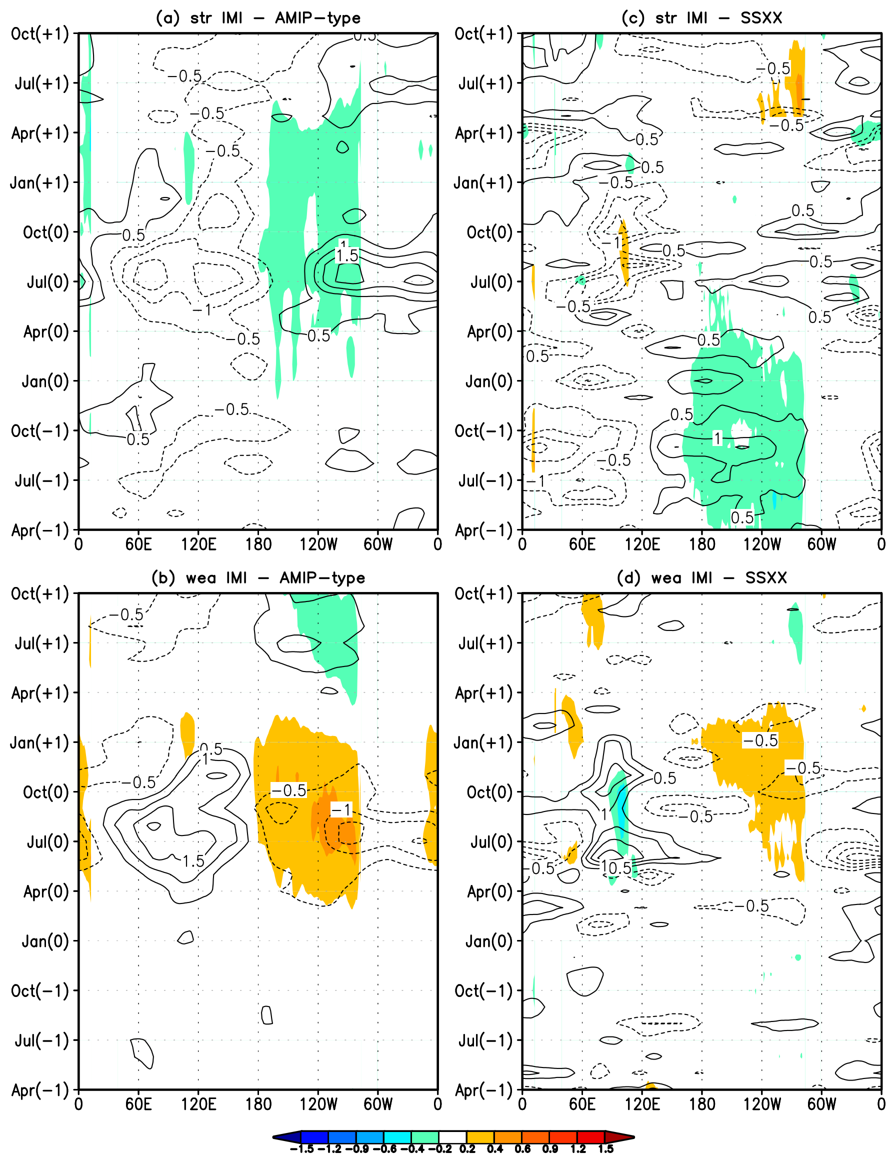


**Fig. 7.** 3-years composite of SST (°C, shaded) and 200 mb velocity potential ($\times$ 1.e+6 1/s$^2$, contours) anomalies averaged between 10S and 10N. The values shown are computed as strong and weak monsoon years composites for (a,b) AMIP-type ensemble and (c,d) coupled model experiment (SSXX). Strong/weak monsoon years are classified based on IMI index.

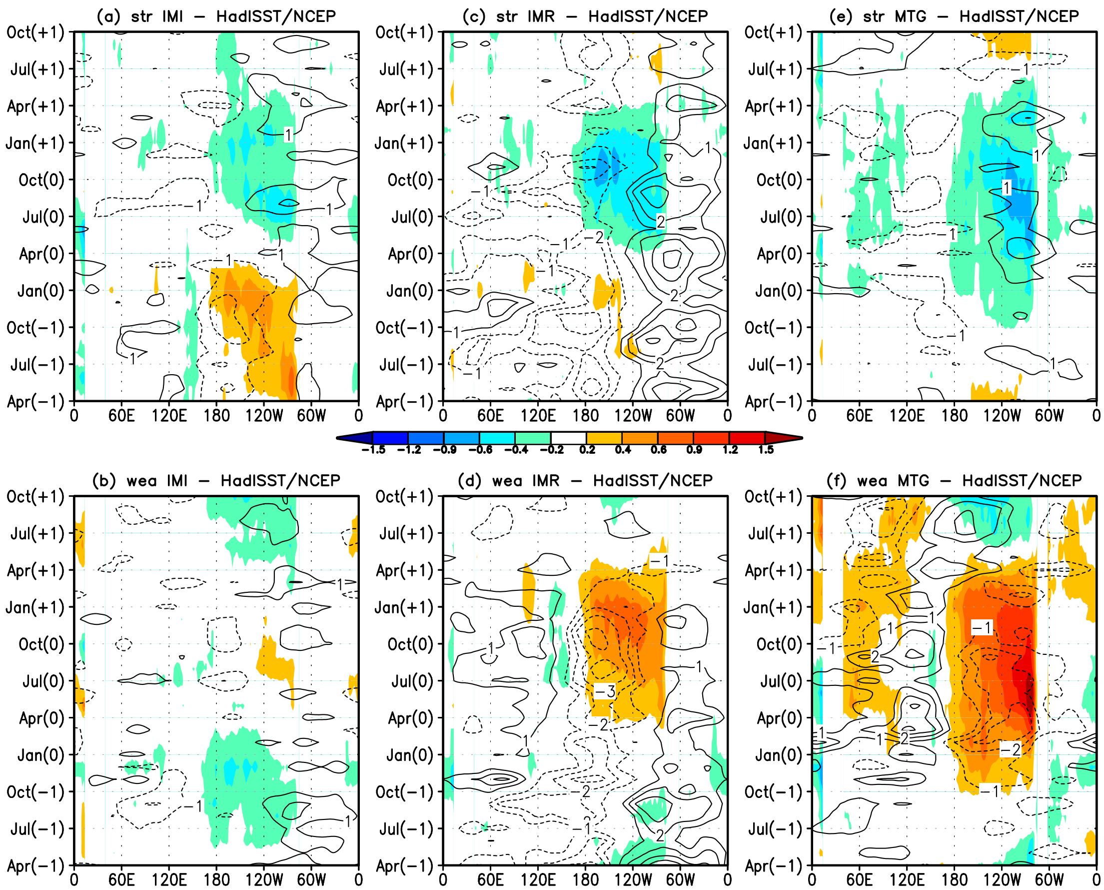


**Fig. 8.** Same as fig. 7, but strong and weak monsoon years are classified based on (a,b) IMI, (c,d) IMR and (e,f) MTG indices in the HadISST and NCEP datasets.

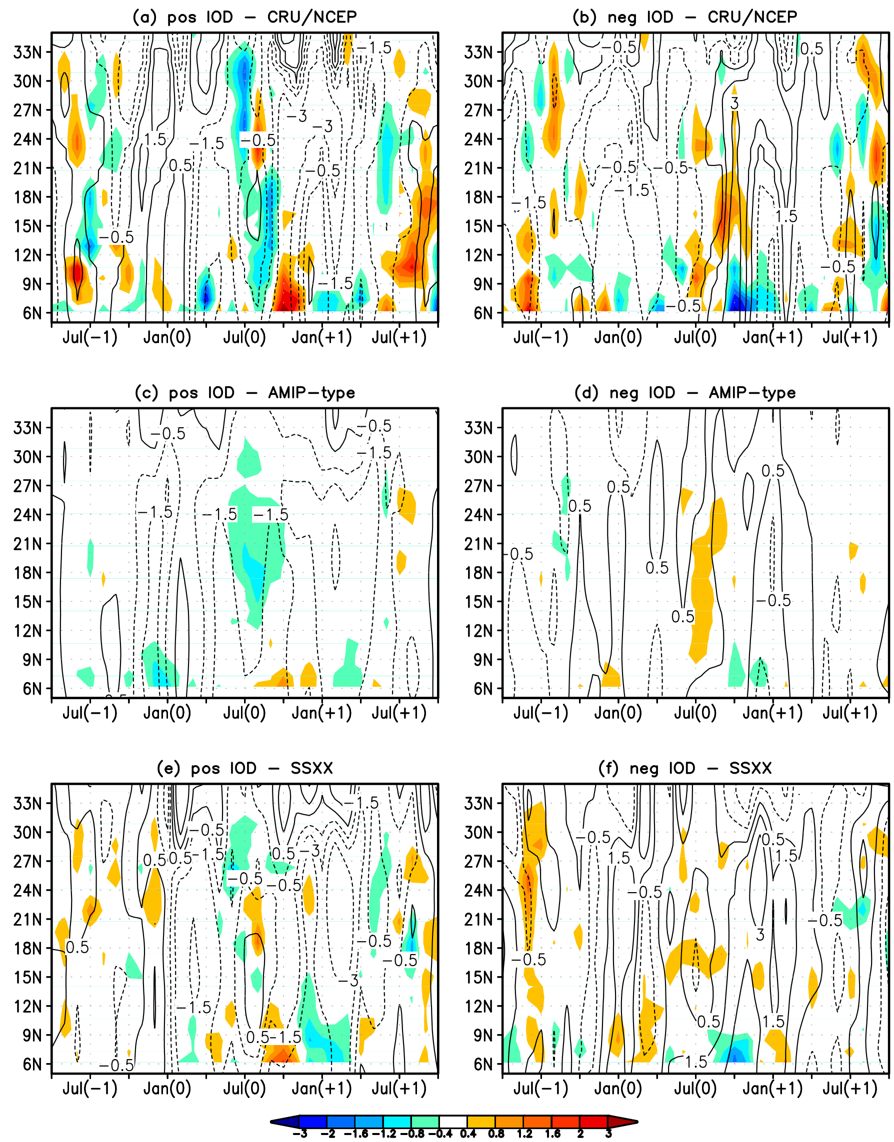


**Fig. 9.** Same as fig. 6, but the composites are computed for positive (left panels) and negative (right panels) IOD events.

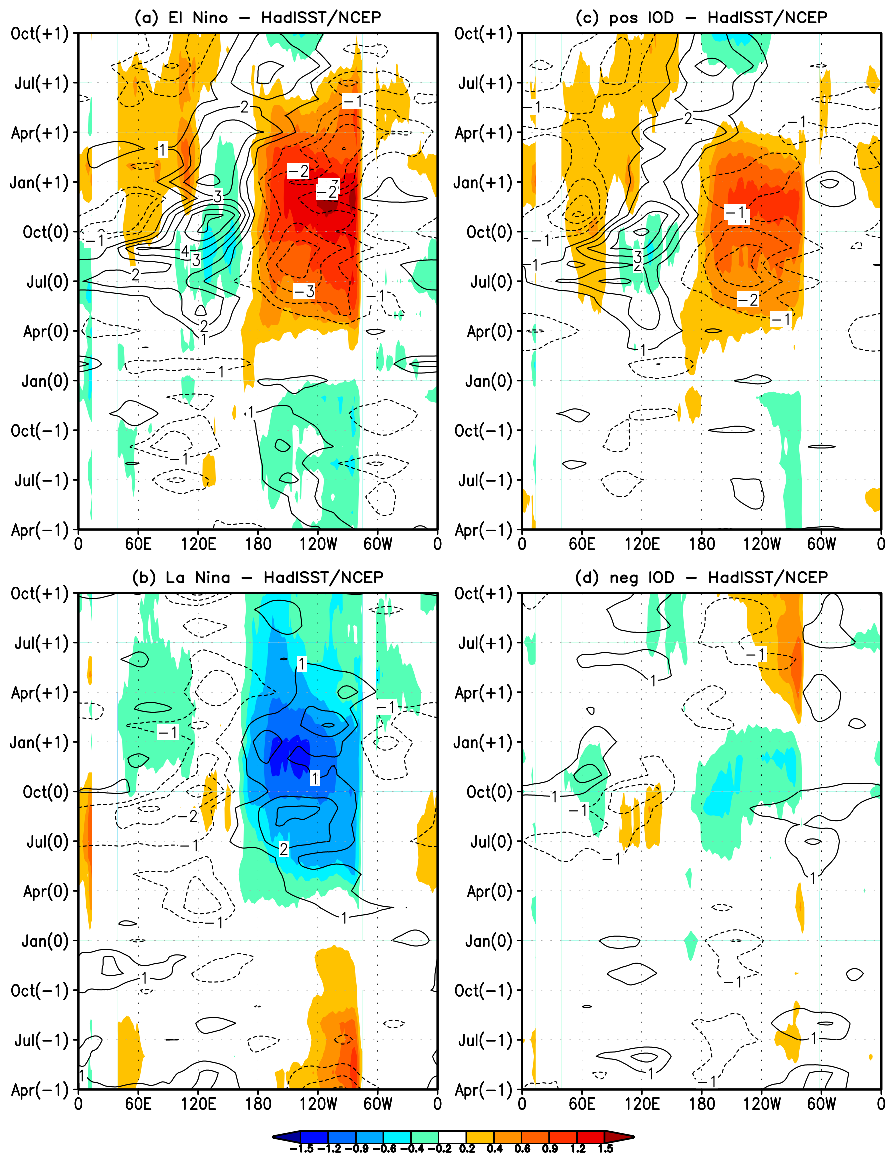


**Fig. 10.** 3-years composite of SST (°C, shaded) and 200 mb velocity potential ($\times$ 1.e+6 1/s$^2$, contours) anomalies averaged between 10S and 10N. The values shown are (a,b) El Niño and La Niña composites and (c,d) positive and negative IOD composites for HadISST and NCEP datasets.

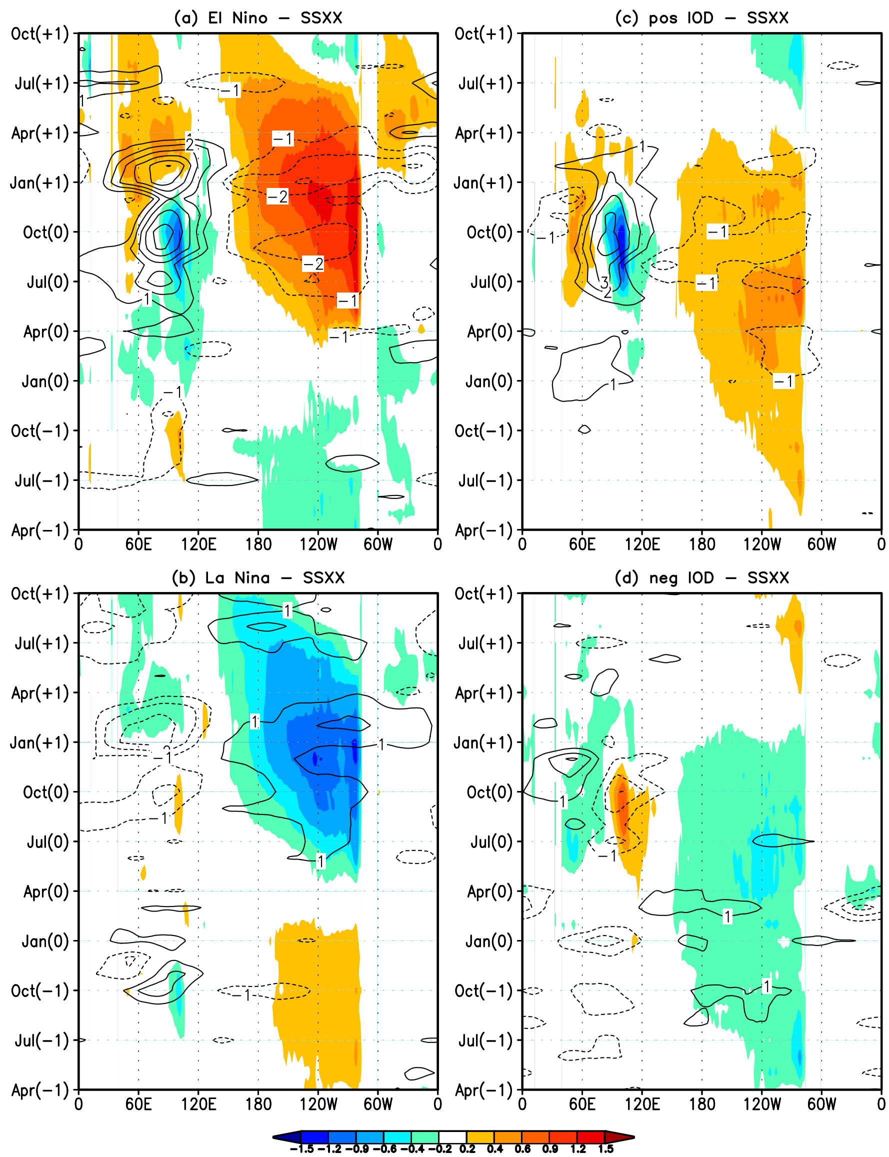


**Fig. 11.** Same as fig. 10, but for the coupled model experiment (SSXX).

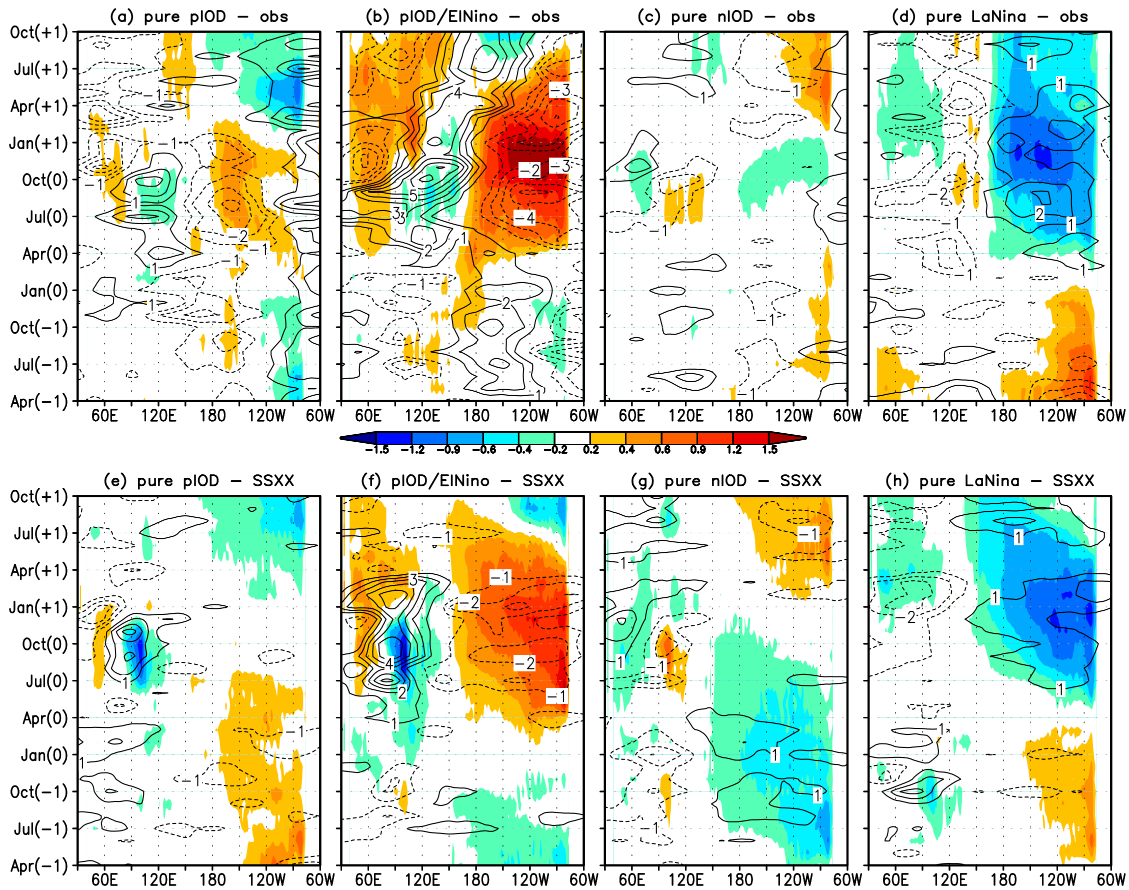


**Fig. 12.** Same as fig. 10, but the values shown are composite of (a,e) pure positive IOD (pure pIOD), (b,f) combined positive IOD and El Niño (pIOD/ElNino), (c,g) pure negative IOD (pure nIOD) and (d,h) pure La Niña (pure LaNina) events in the HadISST and NCEP datasets (upper panels) and in the coupled model experiment (SSXX, lower panels).

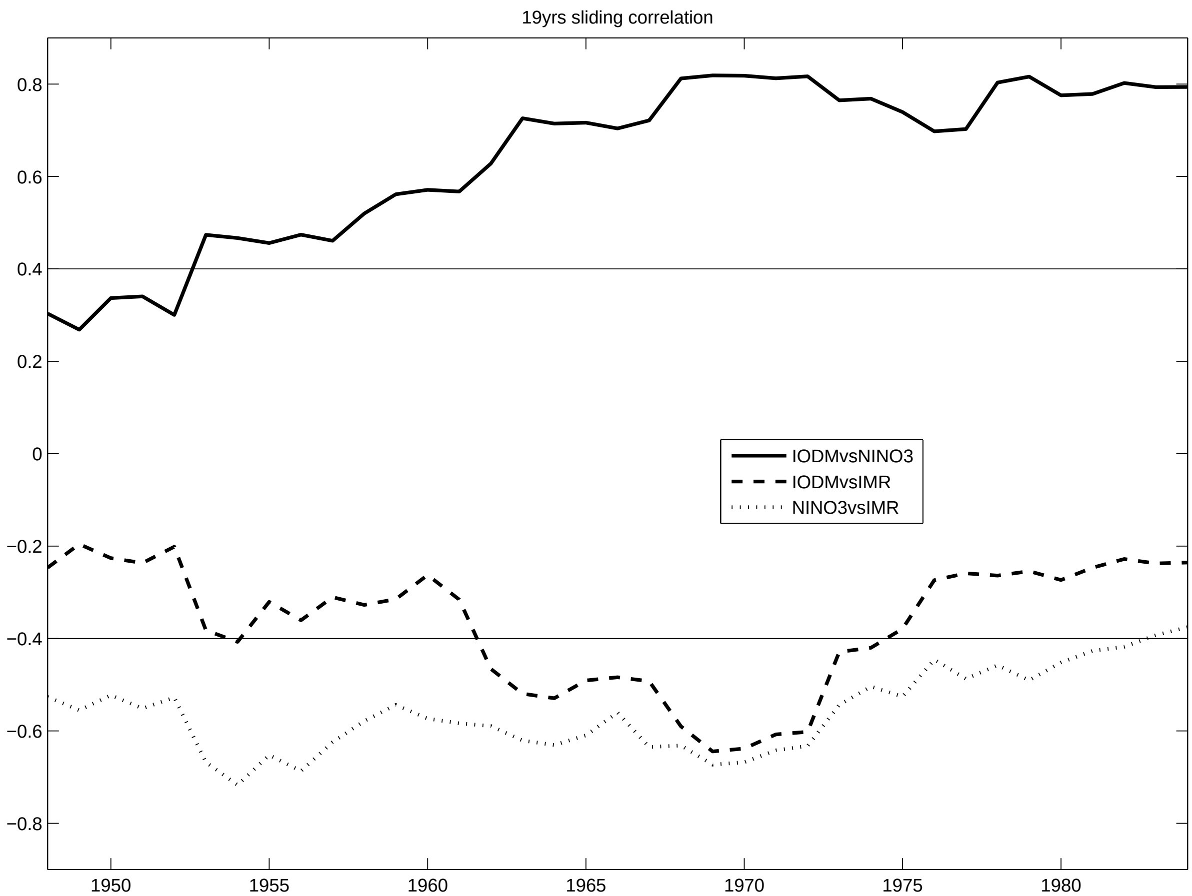


**Fig. 13.** 19 years sliding correlations between IODM and NINO3 (black solid line), IODM and IMR (dashed line), NINO3 and IMR (dotted line) from the CRU and HadISST datasets. Solid horizontal lines indicate the statistical significance threshold at 95%. Years in the x-axis correspond to the starting year of the 19 years correlation window.

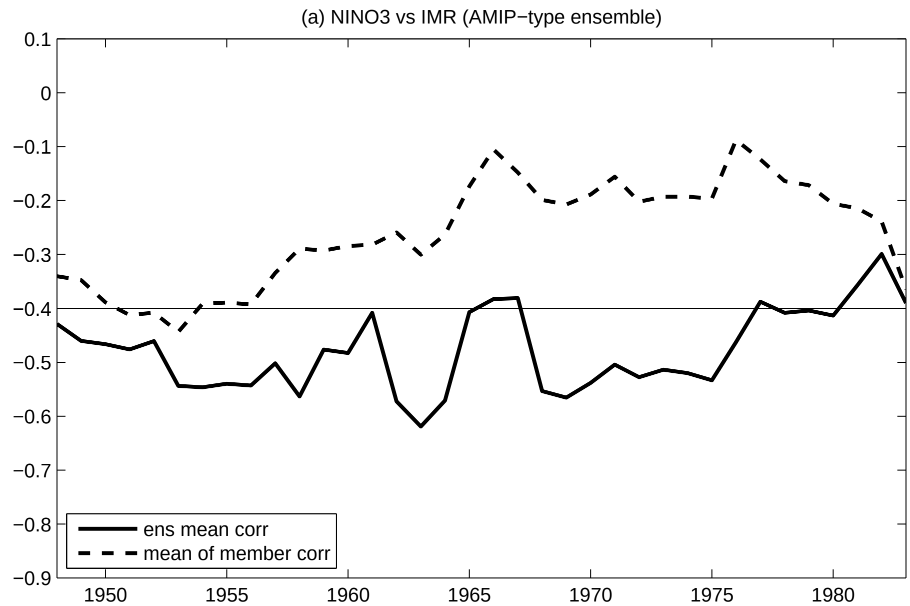


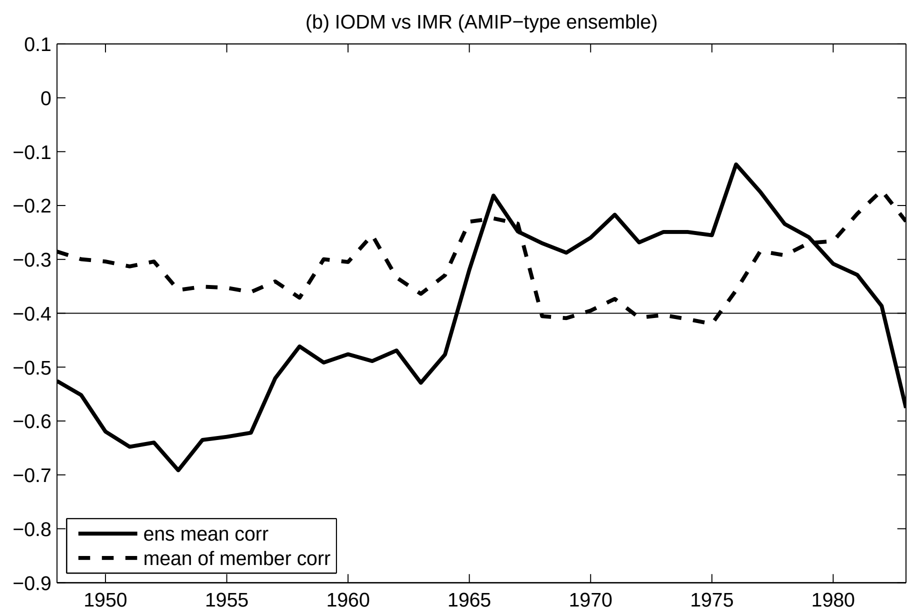


**Fig. 14.** 19 years sliding correlations between (a) NINO3 and IMR and (b) IODM and IMR in the AMIP-type ensemble. In both panels, ensemble mean value (solid line) and the average of the correlation for each member of the ensemble (dashed line) are shown. The solid horizontal line corresponds to the statistical significance threshold at 95%. Years in the x-axis correspond to the starting year of the 19 years correlation window.

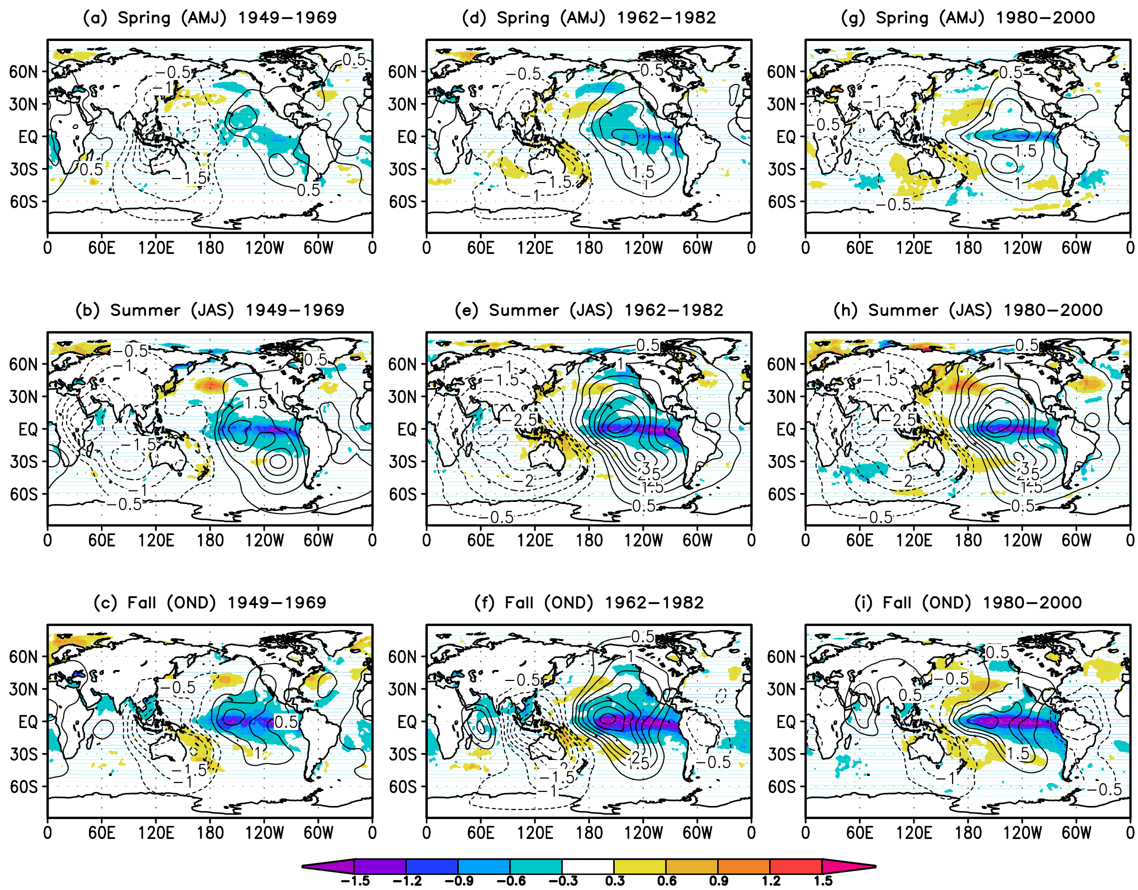


**Fig. 15.** Time-regression of Indian summer monsoon rainfall (IMR) on SST (°C, shaded) and 200 mb velocity potential ($\times$ 1.e+6 1/s$^2$, contours) during spring (AMJ mean, upper panels), summer (JAS mean, middle panels) and fall (OND mean, lower panels) for (a,b,c) 1949-1969, (d,e,f) 1962-1982 and (g,h,i) 1980-2000 time periods.